ApJ, in press (5/8/2012)
Preprint typeset using LaTeX style emulateapj v. 5/2/11

arXiv:1205.2084v1 [astro-ph.SR] 9 May 2012

PLANETS AROUND LOW-MASS STARS (PALMS).
I. A SUBSTELLAR COMPANION TO THE YOUNG M DWARF 1RXS J235133.3+312720*

Brendan P. Bowler,[1,2] Michael C. Liu,[1] Evgenya L. Shkolnik,[3] Trent J. Dupuy,[4,5] Lucas A. Cieza,[1,6] Adam L. Kraus,[1,5] and Motohide Tamura[7]

ApJ, in press (5/8/2012)

ABSTRACT

We report the discovery of a brown dwarf companion to the young M dwarf 1RXS J235133.3+312720 as part of a high contrast imaging search for planets around nearby young low-mass stars with Keck-II/NIRC2 and Subaru/HiCIAO. The 2.″4 (∼120 AU) pair is confirmed to be comoving from two epochs of high resolution imaging. Follow-up low- and moderate-resolution near-infrared spectroscopy of 1RXS J2351+3127 B with IRTF/SpeX and Keck-II/OSIRIS reveals a spectral type of L0^{+2}_{-1}. The M2 primary star 1RXS J2351+3127 A exhibits X-ray and UV activity levels comparable to young moving group members with ages of ∼10-100 Myr. *UVW* kinematics based the measured radial velocity of the primary and the system's photometric distance (50 ± 10 pc) indicate it is likely a member of the ∼50–150 Myr AB Dor moving group. The near-infrared spectrum of 1RXS J2351+3127 B does not exhibit obvious signs of youth, but its *H*-band morphology shows subtle hints of intermediate surface gravity. The spectrum is also an excellent match to the ∼200 Myr M9 brown dwarf LP 944-20. Assuming an age of 50–150 Myr, evolutionary models imply a mass of 32 ± 6 $M_{\rm Jup}$ for the companion, making 1RXS J2351+3127 B the second lowest-mass member of the AB Dor moving group after the L4 companion CD–35 2722 B and one of the few benchmark brown dwarfs known at young ages.

Subject headings: stars: individual (1RXS J235133.3+312720) — stars: low-mass, brown dwarfs

1. INTRODUCTION

M dwarfs are the most abundant denizens of our galaxy and because of their sheer numbers are probably the most common sites of planet formation (Lada 2006). They account for over 70% of stellar systems in the solar neighborhood (Henry et al. 1997) and make up about half of the baryonic mass of our galaxy (Henry 2004). In addition, the single star fraction— a crucial statistic for giant planet formation (e.g., Kraus et al. 2012)— decreases from ∼60-70% for M dwarfs (Fischer & Marcy 1992; Bergfors et al. 2010) to ∼54% for solar-type stars (Duquennoy & Mayor 1991; Raghavan et al. 2010) to near 0% for the most massive stars (Preibisch et al. 1999), further separating M dwarfs from AFGK stars as the most numerous potential planet hosts of all the stellar classes (Lada 2006).

Despite the prevalence of M dwarfs in our galaxy, the population of giant planets orbiting low-mass stars remains poorly understood. At small separations ($\lesssim$3 AU), radial velocity surveys have found that the frequency of giant planets decreases with diminishing stellar host mass (Endl et al. 2006; Johnson et al. 2007; Johnson et al. 2010; Bonfils et al. 2011), a correlation that is consistent with the core accretion model of giant planet formation (e.g., Kennedy & Kenyon 2008). At wide separations (>5 AU), however, there are few observational constraints on the population of gas giants. The statistics from microlensing surveys indicate that a large population of planets exists beyond the snow line of low-mass stars (Gould et al. 2006; Sumi et al. 2010; Gould et al. 2010; Sumi et al. 2011). Recently, Cassan et al. (2012) measured the occurrence rate of 0.3–10 $M_{\rm Jup}$ planets between 0.5–10 AU to be 17^{+6}_{-9}%, with the frequency increasing for lower planet masses. Unfortunately, the host stars from this sample span a large mass range (68% have masses between 0.14 and 1.0 $M_{\odot}$) and their metallicities are unconstrained, so it is unclear how these parameters might influence planet formation at these separations.

Direct imaging offers another approach to study planetary systems at wide separations. This method has several advantages over other planet-finding techniques: it enables detailed studies of regions $\gtrsim$10 AU, and follow-up photometry and spectroscopy of discoveries can be used to study the atmospheres of young giant planets. Yet M dwarfs are conspicuously rare targets of direct imaging surveys due in part to a dearth of known low-mass members of nearby young moving groups (e.g., Shkolnik et al. 2009; Shkolnik et al. 2011; Schlieder et al. 2012). Most deep adaptive optics imaging programs have therefore

---

bpbowler@ifa.hawaii.edu
[1] Institute for Astronomy, University of Hawai‘i; 2680 Woodlawn Drive, Honolulu, HI 96822, USA
[2] Visiting Astronomer at the Infrared Telescope Facility, which is operated by the University of Hawai‘i under Cooperative Agreement no. NNX-08AE38A with the National Aeronautics and Space Administration, Science Mission Directorate, Planetary Astronomy Program
[3] Lowell Observatory, 1400 W. Mars Hill Road, Flagstaff, AZ 86001
[4] Harvard-Smithsonian Center for Astrophysics, 60 Garden Street, Cambridge, MA 02138
[5] Hubble Fellow
[6] Sagan Fellow
[7] National Astronomical Observatory of Japan, 2-21-1 Osawa, Mitaka, Tokyo 181-8588, Japan

* Some of the data presented herein were obtained at the W.M. Keck Observatory, which is operated as a scientific partnership among the California Institute of Technology, the University of California and the National Aeronautics and Space Administration. The Observatory was made possible by the generous financial support of the W.M. Keck Foundation.

focused on the more abundant solar- and high-mass members of these groups, which has lead to increasingly tighter statistical constraints on the population of massive planets on wide orbits around FGK stars (Lafrenière et al. 2007; Biller et al. 2007; Nielsen et al. 2008; Nielsen & Close 2010; Chauvin et al. 2010). M dwarfs are therefore the neglected majority: they are the most common stellar type but our understanding of giant planet formation is the weakest in this stellar mass regime.

To address these disproportionate statistics we are carrying out the Planets Around Low-Mass Stars (PALMS) survey, a high contrast adaptive optics (AO) imaging search for giant planets around nearby ($\lesssim$30 pc) young ($\lesssim$300 Myr) M dwarfs using the Keck-II and Subaru telescopes. Our goals are to find young giant planets and brown dwarf companions to study the atmospheres of these rare low-gravity objects and measure the frequency and mass-period distributions of gas giants orbiting M dwarfs. Our sample of $\sim$70 northern targets originates from ongoing searches for nearby young M dwarfs using the *ROSAT* and *GALEX* all-sky surveys (Shkolnik et al. 2009; Shkolnik et al. 2011). High resolution optical spectroscopy has been used to rule out spectroscopic binarity, identify spectroscopic indicators of youth like Li absorption and gravity-sensitive features, and measure radial velocities. Many of the targets in our sample have been kinematically tied to young moving groups (YMGs) with ages between 10 and 100 Myr (Shkolnik et al. 2012, submitted). Recently, several studies have found that M dwarfs hosting close-in giant planets are preferentially metal-rich (e.g., Johnson & Apps 2009; Rojas-Ayala et al. 2010; Terrien et al. 2012). On average, our sample of young stars is expected to be slightly metal-rich as a result of galactic chemical enrichment over time. Our PALMS survey therefore complements ongoing radial velocity planet searches that are uncovering gas giants around metal-rich field M dwarfs. Finally, we note that only a handful of giant planets have been detected around M dwarfs (7 with masses $> 1\ M_{\rm Jup}$ from radial velocity and microlensing searches; see the compilation in Bonfils et al. 2011), so even a single discovery from our survey is significant.

A handful of planets have now been directly imaged and many more are expected to be discovered with the next generation of specialized planet-finding instruments (i.e., Gemini Planet Imager, Macintosh et al. 2006; HiCIAO+SCExAO, Martinache & Guyon 2009; P1640+PALM-3000, Hinkley et al. 2011; VLT-SPHERE, Beuzit et al. 2008). Many of our expectations about the atmospheric properties of giant planets are shaped by detailed studies of their higher-mass analogs, the brown dwarfs. With similar radii and effective temperatures to young gas giants, brown dwarfs provide empirical spectral sequences across a range of gravities and metallicities. They also serve as tests of substellar atmospheric and evolutionary models, which are the same models used to infer the physical properties of giant planets. The best calibrators are the rare class of benchmark brown dwarfs with known ages and metallicities which can be found as members of coeval clusters (e.g., Lodieu et al. 2008; Rice et al. 2010) or companions to well-characterized stars (e.g, Liu et al. 2002; Luhman et al. 2007; Dupuy et al. 2009; Wahhaj et al. 2011; Crepp et al. 2011).

Here we present the first discovery from our PALMS survey: a substellar companion to the young M2 dwarf 1RXS J235133.3+312720 (hereinafter 1RXS J2351+3127 A). This young star was first identified by Riaz et al. (2006) and Shkolnik et al. (2009) from its large fractional X-ray flux. Shkolnik et al. (2012, submitted) and Schlieder et al. (2012) independently find it to be a likely member of the AB Dor YMG based on its high energy emission and kinematics. Our discovery of a substellar companion to 1RXS J2351+3127 A makes it an important benchmark system at a little-studied age of brown dwarf evolution (Figure 1).

2. OBSERVATIONS

2.1. *PALMS Observing Strategy*

The overall strategy of our survey consists of vetting close visual binaries from our sample and obtaining deep imaging of single young M dwarfs. Binaries are removed for several reasons: (1) moderate-separation binaries ($\lesssim$40 AU) are likely disruptive to giant planet formation as a result of rapid disk dispersal (Kraus et al. 2012); (2) for giant planets forming in circumbinary disks, very tight binaries can be approximated as single point masses made of the total mass of the binary pair, and therefore cannot be included in our final statistical analysis which is focused on low stellar masses; and (3) wavefront correction in adaptive optics systems is generally optimized for single point sources, so binaries will tend to reduce image quality and lower Strehl ratios. Our deep coronagraphic imaging of each target is conducted in angular differential imaging (ADI) mode (e.g., Liu 2004; Marois et al. 2006); these data will be discussed in a future publication.

2.2. *Keck-II/NIRC2 NGS AO Imaging*

We imaged 1RXS J2351+3127 AB with Keck-II/Near Infrared Camera 2 (NIRC2) coupled with natural guide star (NGS) adaptive optics (Wizinowich et al. 2000) on 21 June 2011 UT and 15 November 2011 UT. The narrow camera setting was used for both epochs, resulting in a field of view of $10''.2\times10''.2$. Our June 2011 data were obtained at an airmass of 1.17 with the MKO H-band filter (Simons & Tokunaga 2002; Tokunaga & Vacca 2005). We first acquired short unsaturated images of the primary (reading out the central 192×248 pixels instead of the full 1024×1024 array) for photometric calibration and to check for binarity. We then obtained five 10 sec images using the full array with 1RXS J2351+3127 A placed behind the $0''.6$ diameter translucent focal plane mask; 1RXS J2351+3127 B is clearly visible in individual frames (Figure 2). Conditions were photometric and the Differential Imaging Motion Monitor on CFHT reported $0''.4$ seeing during the observations. Second epoch imaging in November 2011 was performed in the K'-band filter at an airmass of 1.05. Nine short (0.2 sec) non-coronagraphic frames of 1RXS J2351+3127 AB were acquired during excellent ($\sim0''.5$) conditions. Our imaging data are summarized in Table 1.

Cosmic ray and bad pixel removal, dark subtraction, and flat fielding were performed on each image. The coronagraphic frames suffer from dust features present on the focal plane slide which contains the occulting spot. This slide may not return to exactly the same position with each new setup, so we created two flat frames to remove normal detector and optical inhomogeneities as well as residual dust features from this nonstatic optical component. We obtained dome flats with and without the mask, then generated a "coronagraph" flat by dividing the normal dome flat. After masking out the occulting spot from the coronagraph flat (that is, the region centered on the coronagraph spot was set to unity), we matched the flat to the image through cross correlation, then divided it into the image. Optical distortions were corrected using the distortion solution made available by the Keck Observatory, which was developed by B. Cameron and is accurate to ∼0.2-0.3 pix across the entire image (Yelda et al. 2010).

Our H-band coronagraphic data preceeded deep angular differential imaging (which will be presented in a future publication) so the image rotator was turned off for the observations (i.e., the rotator was in"vertical angle mode"), causing 1RXS J2351+3127 B to rotate about the primary by 0.34° during the short sequence. The images were registered by fitting a 2D elliptical Gaussian to the primary star behind the coronagraph and derotated to a common position angle using a cubic convolution interpolation. North alignment was performed using keywords stored in the FITS header, taking into account the offset between the AO and NIRC2 detector (+0.7°) and the sky orientation on the detector of $+0.252 \pm 0.009°$ derived by Yelda et al. (2010).

Astrometry was measured for each image using centroid positions of 1RXS J2351+3127 A and B and the NIRC2 plate scale of 9.952 ± 0.002 mas pix^{-1} from Yelda et al. (2010). Errors in the separation and position angle (PA) were computed from Monte Carlo realizations taking into account uncertainty in the North angle alignment, plate scale, centroid position (assumed to be 0.1 pix), and distortion solution (0.3 pix). The adopted values for each epoch are weighted averages from the individual frames. (The uncertainties in separation and PA from individual images are roughly 4 mas and 0.1°, respectively.) Our measurements are summarized in Table 2.

We computed flux ratios for our H-band data using the short images of the primary and the longer 10 sec coronagraphic frames where the companion is visible. We performed aperture photometry at the centroided positions of both components using an aperture radius of 10 pix and annular sky subtraction, arriving at an H-band flux ratio 5.68 ± 0.04 mag and a K'-band flux ratio of 5.04 ± 0.05 mag.

2.3. *IRTF/SpeX Prism Near-Infrared Spectroscopy*

We obtained a low-resolution 0.8–2.5 μm spectrum of 1RXS J2351+3127 B with IRTF/SpeX (Rayner et al. 2003) in prism mode on 14 October 2011 UT. The $0\farcs3$ slit was used (2 pixels per resolution element), resulting in an average resolving power ($R \equiv \lambda/\Delta\lambda$) of ∼250 across the spectrum. Atmospheric conditions were good during the observations (DIMM on CFHT reported $0\farcs5$ seeing) with some light cirrus. The slit was oriented perpendicular to the binary PA; although this differed from the parallactic angle, differential chromatic refraction was negligible because of the low airmass (sec$z$=1.1). A total of 12 min of data were obtained by nodding along the slit in an ABBA pattern (Table 1). Immediately afterward we observed the A0V standard HD 222749 for telluric correction at a similar airmass (sec$z$=1.2) and position on the sky. Internal flats and arc frames were taken for flat fielding and wavelength calibration. The spectra were extracted, median-combined, and corrected for telluric features using the IDL package Spextool (Cushing et al. 2004; Vacca et al. 2003). The median S/N per pixel between 0.8–2.5 μm is 74 and reaches over 130 in J band.

The spectrum of 1RXS J2351+3127 B suffers from significant contamination from the primary at $\lambda \lesssim 1.2$ μm, which was evident in the pair-subtracted images. However, the smaller PSF FWHM at longer wavelengths resulted in a better separation at H- and K-bands, so contamination should be negligible in those regions. We flux calibrated the spectrum using the K-band photometry from Keck and the conversion to the MKO system described in Section 3.2.

2.4. *IRTF/SpeX SXD Near-Infrared Spectroscopy*

We observed 1RXS J2351+3127 AB with the IRTF/SpeX spectrograph in short cross-dispersed mode (SXD) on 2 Dec 2011 UT. Conditions were excellent with DIMM on CFHT reporting $0\farcs4$ seeing. We used the $0\farcs5$ slit ($R \sim 1200$) oriented at the binary position angle so that both the primary and companion were observed. The observations were taken in an ABBA pattern over an airmass range from 1.02 to 1.06. We obtained 24 120-sec exposures, resulting in a total on-source integration time of 48 min. The A0V star 7 Tri was then targeted for telluric correction, and calibration frames were taken at the same telescope position.

The data were reduced with Spextool. It was clear from the collapsed spatial profiles of each order that the wing of the point spread function from the primary overlapped with the companion. Like in the prism data, the system was better separated at H and K because of the smaller FWHM, but contamination became progressively worse at $\lesssim 1.1$ μm. As a result, we processed the spectra of the companion without optimal extraction and sky subtraction, and we limited the extraction to orders 3, 4, and 5 (K, H, and J bands, respectively, or 1.1–2.5 μm). The SXD spectrum appears to be slightly redder than the prism spectrum, which may indicate there is less contamination. (The synthetic J–K (MKO) colors of the SXD and prism spectra are 1.26 mag and 1.17 mag.) The 4th order of the companion fell on a region of the detector where a faint ghost exists. Consequently, a large artifact was present in the reduced spectrum between 1.71–1.75 μm, so we removed this spectral region. The extraction of the primary star and the standard were performed the usual way with Spextool using optimal extraction and background subtraction. The median S/N per pixel of the companion spectrum is 26 and is over 40 in H and K.

2.5. *IRTF/SpeX Guider Camera YJHK Imaging*

We obtained additional relative photometry of 1RXS J2351+3127 AB with the guider camera on IRTF/SpeX on 2 Dec 2011 UT. We imaged the system in the Y,[9] J, H, and K_S filters in nodded patterns. The details of our observations are listed in Table 1. Each frame was corrected for bad pixels and cosmic rays, pair subtracted, and divided by a flat frame created from the science data after masking out the system. The images were then registered and stacked to extract relative photometry. The companion is clearly visible in all filters and sits in the wing of the primary's PSF (Figure 3). We performed relative photometry by modeling each PSF as the sum of three elliptical Gaussians as described in Liu et al. (2010a). Uncertainties were computed by inserting and extracting artificial companions at same separation as the real object but different PAs. The artificial companion was created by scaling the primary star to the same brightness as the real companion. The resulting photometry is presented in Table 3, where quoted uncertainties represent the standard deviation of several hundred realizations of this process. Our IRTF K-band photometry disagrees with our Keck measurements by $\sim$4-σ. Since the PSFs overlap in our IRTF data this discrepancy is probably a result of a slight systematic error or underestimated measurement uncertainty in our IRTF photometry. We emphasize that while our IRTF data were obtained in excellent seeing conditions, our photometry and spectroscopy of the companion may contain minor systematic errors as a result of its close proximity to the primary star. Our Keck data taken with adaptive optics is expected to be much more reliable.

---

[9] This filter is labeled "Z" in the Guidedog GUI and instrument documentation, but with a bandpass of 0.95–1.11 μm it better resembles the Y filter described in Hillenbrand et al. (2002).

2.6. *Keck-II/OSIRIS J-Band Spectroscopy*

On 26 Dec 2011 UT we obtained Keck-II NGS-AO 1.18–1.35 μm spectroscopy of 1RXS J2351+3127 B with the OH-Suppressing Infrared Imaging Spectrograph (OSIRIS; Larkin et al. 2006). Unlike our IRTF/SpeX data, the combination of adaptive optics and an integral field unit enables resolved spectroscopy of the companion without contamination from the primary star. We obtained three nodded pairs with exposures of 300 sec per position with the *Jbb* filter and the 50 mas plate scale, totaling 30 min of on-source data (Table 1). The resulting field of view was $0\farcs8\times3\farcs2$ and the resolving power was $\sim$3800. Immediately following our science observations we targeted the A0V star HD 78215 to correct for telluric features.

The data were reduced with the OSIRIS data reduction pipeline[10] and the latest rectification matrix made available by the Keck Observatory. Nodded pairs were used for mutual sky subtraction. The spectra were extracted from the data cubes using 3 pix (150 mas) circular apertures. The individual spectra were first scaled to a median-combined spectrum, then deviant pixels were removed with a sigma-clipping algorithm at each wavelength using a 3 σ threshold, and finally the spectra were combined by computing mean and standard errors at each wavelength. Telluric correction was performed with the `xtellcor_general` routine in the Spextool spectroscopic reduction package. At its native resolution the final spectrum has a median S/N per pixel of $\sim$15.

3. RESULTS

3.1. *Common Proper Motion*

We use the sky coordinates, distance estimate (50 ± 10 pc, see Section 3.2), and proper motion of 1RXS J2351+3127 A along with first epoch astrometry of the candidate companion to predict the separation and position angle (or, equivalently, change in right ascension and declination) of a distant background object over time. The results are shown in Figure 4, with shaded errors at each epoch incorporating uncertainties in distance, proper motion, and first epoch astrometry. Our second epoch Keck astrometry is consistent with our first epoch measurements (within 3-σ) and rules out the background hypothesis at 7-σ, proving the companion is comoving and very likely gravitationally bound to the primary. The second epoch separation is indistinguishable from the expected separation of a background object, but the position angle of a background object differs from the second epoch measurement by 0.99 ±0.13 deg. Most of the uncertainty in this value is from the error in the background model PA at that epoch rather than the measured PA of the companion.

3.2. *Distance*

There are several distance estimates to the primary star 1RXS J2351+3127 A in the literature. Reid et al. (2007) use absolute magnitude-optical band strength index relations (M_J-TiO5 and M_J-CaH2) to arrive at an estimated M_J of 7.08 ± 0.34 mag and a corresponding distance of 35.0 ± 5.6 pc. Riaz et al. (2006) use a slightly different M_J-TiO5 relation and arrive at a distance of 50 pc (we calculate an uncertainty of 20 pc using the quoted rms from their relation.) Both estimates make use of field relations and assume the star is single. Recently Schlieder et al. (2012) estimated a kinematic distance of 41.3 ±3.2 pc for 1RXS J2351+3127 A using the technique described in Lépine & Simon (2009), which assumes it is a member of the AB Dor YMG (see Section 3.3.3).

The late-type companion can also be used to obtain an independent distance estimate for the system. The most extensive compilation of field MLT objects with parallaxes was recently assembled by Dupuy & Liu (2012). They measure an $M_{K_{\rm MKO}}$ value of 10.46 ± 0.15 for L0 objects, which is the spectral type we adopt for 1RXS J2351+3127 B (Section 3.4). Our K' contrast measurement must first be converted to $K_{\rm MKO}$ to use this relation. The synthetic $K_{\rm MKO}$-K' and K_S-K' colors from our SXD spectrum of 1RXS J2351+3127 A are $<$ 0.02 mag, so we assume $K_{\rm MKO}{\sim}K'{\sim}K_S$ for the primary. Our prism spectrum of the companion yields a $K_{\rm MKO}$-K' color of –0.09. Taking this into account and using the 2MASS magnitude of the primary gives a $K_{\rm MKO}$-band magnitude of 13.92 ± 0.05 mag and a distance of 49 ± 5 pc.

If the system is young then field relations will underestimate the objects' luminosities and distances. Assuming instead an age comparable to the Pleiades ($\sim$120 Myr), we can make use of photometry of known late-type Pleiades members to infer an empirical *SpT*-absolute magnitude relation for young objects. Isolating Pleiades members from Bihain et al. (2006) with spectral types between M9 and L1 and using a cluster distance of 133 pc (Soderblom et al. 2005) yields an average $M_{K_{\rm MKO}}$ value of 10.0 ±0.6 mag and a slightly larger distance of 60 ± 17 pc for 1RXS J2351+3127 B. Altogether we adopt a distance of 50 ± 10 pc, with a younger age favoring a larger distance.

---

[10] Version 2.3: http://irlab.astro.ucla.edu/osiris/.

3.3. *Age*

3.3.1. *X-ray Activity*

Low-mass stars have long been known to exhibit age-rotation-activity relationships spanning their pre-main sequence and main sequence lifetimes (Skumanich 1972). They are born with high angular momenta and fast rotation rates, which induce strong magnetic fields and result in active coronal and chromospheric emission (e.g., Feigelson & Montmerle 1999; West et al. 2008). Angular momentum loss through stellar winds slows rotation and diminishes magnetic field strengths over time (Feigelson et al. 2004; Barnes & Kim 2010; Reiners & Mohanty 2012). Observationally this manifests as an evolution of rotation rates (e.g., Irwin et al. 2011) and X-ray activity (e.g., Preibisch & Feigelson 2005); both are calibrated to young coeval clusters and old field stars but have considerable dispersion for a given age and stellar mass.

1RXS J2351+3127 A was first identified in a large spectroscopic survey by Riaz et al. (2006) to locate new nearby M dwarfs using a combination of 2MASS and the *ROSAT* All Sky Survey catalogs. They found a high fractional X-ray luminosity of log $L_X/L_{\rm Bol} = -3.02$, which corresponds to the saturation limit for low-mass stars (e.g., Delfosse et al. 1998; Pizzolato et al. 2003; Wright et al. 2011). How does this compare to typical values for young clusters? Preibisch & Feigelson (2005) present a comprehensive analysis of the evolution of X-ray activity for various stellar mass bins between the ages of ∼1 Myr and several Gyr. Fractional X-ray luminosities decline over time, but less precipitously for low-mass stars compared to solar-type stars. The median values for 0.1–0.5 $M_\odot$ stars only decrease by ∼0.4 dex from the 1-10 Myr clusters to Hyades ages (∼625 Myr), whereas 0.9–1.2 $M_\odot$ stars vary by ∼1.7 dex over the same timeframe. Both stellar mass bins show a subsequent drop of ∼1.3 dex from the Hyades to the field age. The fractional X-ray luminosity for 1RXS J2351+3127 A is well above typical values of even the youngest clusters. The cumulative distributions for low-mass stars (0.1-0.5 $M_\odot$) from Preibisch & Feigelson (2005) indicate that even the most active tail of field objects never reaches values of –3.0, although a more precise age determination is difficult using log $L_X/L_{\rm Bol}$ alone since the distributions for young clusters overlap.

The cumulative distributions of X-ray luminosities (log L_X) from Preibisch & Feigelson (2005) are somewhat less degenerate than for fractional X-ray luminosities. Using the count rate to flux conversion factor from Fleming et al. (1995) and assuming a distance of 50 ± 10 pc yields log L_X=29.3 ± 0.2 erg/s for 1RXS J2351+3127 A. In Figure 5 (left panel) we compare this to the distribution of luminosities for various populations from Preibisch & Feigelson (2005). 1RXS J2351+3127 A is consistent with the ONC, Pleiades, and the most X-ray luminous members of the Hyades, but is inconsistent with field objects.

The *ROSAT* Position Sensitive Proportional Counter (PSPC) instrument had modest energy resolution, enabling a rough measurement of the X-ray spectrum using hardness ratios as defined in Voges et al. (1999). Stellar X-ray emission softens with age as a result of decreasing absorption by foreground gas at very early ages ($\lesssim$10 Myr; Neuhäuser et al. 1995) and an evolving coronal gas temperature at intermediate and old ages (∼10 Myr–10 Gyr; Kastner et al. 2003), so hardness ratios can be used as a crude indicator of age. For a comparison sample we searched the RASS Bright Source Catalog (Voges et al. 1999) for X-ray counterparts within 40″ of stars in two age bins: Upper Scorpius members (∼5 Myr) from Preibisch & Mamajek (2008); and AB Dor, β Pic, Columba, Tuc-Hor, and TWA YMG members (∼10-100 Myr) from Torres et al. (2008). In addition, we use the NEXXUS 2 catalog (updated from Schmitt & Liefke 2004; C. Liefke, private communication) for an older sample (∼1-10 Gyr) of field stars with RASS detections, limiting distances to <15 pc. Figure 6 shows the resulting HR1/HR2 distributions; USco members have very hard HR1 values near 1.0, the intermediate age sample has HR1 values between ∼–0.4 and +0.3, and field M dwarfs have values between ∼–0.5 and 0.0. The hardness ratio of 1RXS J2351+3127 A (HR1=-0.33 ±0.16) is consistent with both YMG members and M dwarfs in the field.

We also compute X-ray luminosities for the USco, YMG, and field populations and show the log L_X vs. HR1 distributions in Figure 5 (right panel). Note that not all of queried objects had X-ray counterparts, and since the RASS is a flux-limited survey the samples and distributions for each age group represent the most X-ray luminous members of each population. Deeper pointed observations of young compact clusters show a much larger spread in X-ray luminosities at a given age, spanning, for example, almost 3 orders of magnitude for the ∼1 Myr ONC cluster (Preibisch & Feigelson 2005). (These results also suggest that all-sky searches which require X-ray detections to identify nearby young stars are missing a large fraction of young X-ray-faint members.) The X-ray luminosity of 1RXS J2351+3127 A appears to be inconsistent with field M dwarfs, agreeing better with young moving group members which have ages of ∼10-100 Myr.

Shkolnik et al. (2009) and Schlieder et al. (2012) compute fractional X-ray fluxes for their samples of X-ray selected targets and derive values of log F_X/F_J = –2.23 and log F_X/F_{K_S}=–2.06, respectively, for 1RXS J2351+3127 A. Both values lie near the saturation limit for early M dwarfs and are comparable to YMG members with ages less than the Pleiades (∼120 Myr). Shkolnik et al. (2009) obtained two epochs of high resolution spectroscopy of 1RXS J2351+3127 A and rule out spectroscopic binarity as the source of increased activity. They also found a CaH band strength suggesting low surface gravity but did not detect Li, leading to a a likely age of 20-150 Myr.

3.3.2. *UV Activity*

Chromospheric activity produces a wealth of emission lines and continuum flux at UV wavelengths (e.g., Robinson et al. 2005; Pagano 2009). This activity decays over time (Simon et al. 1985; Ribas et al. 2005; Findeisen et al. 2011), making excess UV emission a good tracer of magnetic field strength and age. The *Galaxy Evolution Explorer* (*GALEX*; Martin et al. 2005) space telescope mapped most of the sky in near-UV (NUV) and far-UV (FUV) bands and the resulting catalog (Morrissey et al. 2007) represents a rich resource to identify nearby young stars that exhibit UV excesses (Shkolnik et al. 2011; Rodriguez et al. 2011; Schlieder et al. 2012).

1RXS J2351+3127 A was detected in both *NUV* and *FUV* bands of *GALEX* (Table 3). Here we compare its UV emission to several empirically calibrated UV/near-infrared colors from the literature. 1RXS J2351+3127 A exhibits high fractional UV fluxes relative to its J-band and K_S-band fluxes with values consistent with local association members (Shkolnik et al. 2011; Schlieder et al. 2012). Rodriguez et al. (2011) find distinct loci for field and YMG populations in both NUV–V vs. V–K and NUV–J vs. J–K planes. Lacking a reliable V-band magnitude for 1RXS J2351+3127 A, we can use the typical V–K color for an M2V dwarf of 4.11 mag (Tokunaga 2000) to provide an estimate. Combining this with the 2MASS K_S-band magnitude of 1RXS J2351+3127 A yields a value of V=13.1 mag. Comparing its NUV–V color of ∼6.9 mag to Figure 2 of Rodriguez et al. shows that 1RXS J2351+3127 A is clearly discrepant from the field population and again sits along the locus of YMG objects. Likewise, its NUV–J color (10.15 mag) is ∼1.5 magnitudes bluer than the field population for its J–K_S color (0.85 mag) based on Figure 4 of Rodriguez et al. It is also bluer than Hyades sequence based on Figure 7 of Findeisen et al. (2011). Although the scatter is quite large, Findeisen et al. (2011) derive an empirical calibration for log(age) vs. FUV–J and J–K colors (their Equation 10), which yields an age of 36^{+53}_{-21} Myr. Altogether, the UV fluxes of 1RXS J2351+3127 A point to an age that is confidently less than the Hyades (625 Myr) and likely between 10-150 Myr.

3.3.3. *Kinematics*

Both Schlieder et al. (2012) and Shkolnik et al. (2012, submitted) independently find that 1RXS J2351+3127 A is a likely member of the AB Dor YMG. Schlieder et al. use the method of Lépine & Simon (2009) to compute a kinematic distance and predict a radial velocity assuming cluster membership. Their kinematic distance for 1RXS J2351+3127 A (41.3 ± 3.2 pc) matches our photometric distance of the system (50 ± 10 pc), and their predicted radial velocity (–14.0 ± 1.3 km/s) is in excellent agreement with the measured value of –13.5 ± 0.6 km/s by Shkolnik et al. The radial velocity of 1RXS J2351+3127 A was measured from two high resolution spectra ($\lambda/\Delta\lambda \sim 68{,}000$) obtained by Shkolnik et al. (2009) on 14 Aug 2006 UT and 5 Oct 2006 UT with the Échelle SpectroPolarimetric Device for the Observation of Stars at the Canada-France-Hawaii Telescope. Details about the measurements will appear in Shkolnik et al. (2012, submitted). In brief, the spectra were cross-correlated with an RV standard with a similar spectral type and the radial velocity was derived from Gaussian fits to the cross-correlation functions.

$UVWXYZ$ values for 1RXS J2351+3127 A with respect to the Sun's space motion and position are listed in Table 4. Given the large range of photometric distances for the system, we also compute space motions for distances of 35, 45, 55, and 65 pc, which are plotted in Figure 7 relative to YMGs from Torres et al. (2008). For distances between ∼35 and 50 pc the kinematics of 1RXS J2351+3127 A agree well with the AB Dor group and sit in the cluster center at ∼45 pc. Distances larger than 55 pc are discrepant with the cluster. Although membership is highly probable, a parallax for the system and verification using cluster convergence-point methods (e.g., Torres et al. 2006; Mamajek 2005; Galli et al. 2012) is essential for unambiguous association.

3.3.4. *Age Summary*

The high X-ray and UV emission from 1RXS J2351+3127 A point to an age significantly younger than the Hyades. A more precise age determination from high energy emission alone is hindered by the large intrinsic scatter from young moving group members. The UVW kinematics of 1RXS J2351+3127 AB based on its photometric distance are consistent with the AB Dor moving group, which has an age comparable to the Pleiades. However, a parallax is required to verify cluster membership. Very young ages ($\lesssim$10 Myr) can be excluded based on the morphology of the near-infrared spectrum of 1RXS J2351+3127 B (Section 3.4) and the lack of Li in the primary. Altogether we adopt two age estimates for 1RXS J2351+3127 AB: 50–150 Myr assuming AB Dor membership, and a conservative estimate of 50–500 Myr if the system does not belong to that cluster.

3.4. *Spectral Properties and Classification*

3.4.1. *Low-Resolution Prism Spectrum*

Our 0.8-2.5 μm SpeX prism spectrum of 1RXS J2351+3127 B shows typical features of late M- and early L-type objects (i.e., deep 1.5 and 1.9 μm steam bands; strong 2.3 μm CO absorption; and (blended) Na I, K I, and FeH features in J-band; Cushing et al. 2005) despite clear and significant contamination from the primary star at $\lambda \lesssim 1.2$ μm (see Section 2.3). Here we attempt to use the uncontaminated (or minimally contaminated) regions of the spectrum for the purposes of spectral classification. Our comparison spectra come from the SpeX Prism Spectral Library.[11] We tried fitting several spectral regions of 1RXS J2351+3127 B to a sample of 618 published M, L, and T dwarf spectra which were also obtained with IRTF/SpeX in prism mode. The χ^2 statistic was used as a goodness-of-fit metric, and we ignored measurement uncertainties in the library spectra.

The best-fitting object to the entire 1.20–2.45 μm region is the intermediate-age M9.0 (optical spectral type) brown dwarf LP 944-20 (Figure 8). Optical spectroscopy of LP 944-20 by Tinney (1998) revealed Li absorption, indicating it is a young substellar object (see also Pavlenko et al. 2007). Follow-up studies uncovered evidence for X-ray flaring (Rutledge et al. 2000), quiescent radio emission (Berger et al. 2001), possible photometric variability (Tinney & Tolley 1999), and optical, but not infrared, periodic radial velocity variations (Martín et al. 2006). All of this indicates that LP 944-20 harbors an unusually strong magnetic field for its spectral type. Ribas (2003) found that LP 944-20 is a likely member of the Castor YMG (which includes the well-studied stars Vega and Fomalhaut) based on its space motion. Age estimates for the Castor YMG range from ∼200–400 Myr

---

[11] Maintained by Adam Burgasser at http://pono.ucsd.edu/∼adam/browndwarfs/spexprism.

(Barrado 1998; Torres & Ribas 2002; Ribas 2003), i.e., intermediate in age between the Pleiades (125 Myr) and the Hyades (625 Myr).

The near-infrared prism spectrum of LP 944-20 itself (Burgasser et al. 2008) reveals only subtle hints of youth. One of the most discriminating features exhibited by young brown dwarfs at low spectral resolution is a triangular-shaped H-band (e.g., Lucas et al. 2001; Allers et al. 2007). This feature is readily seen in Figure 8, which shows the spectrum of LP 944-20 compared to the L0 optical standard 2MASS J0345432+254023 (Burgasser & McElwain 2006) and the young M9.5 TWA brown dwarf 2MASS J11395113–3159214 (Looper et al. 2007). LP 944-20 has an intermediate H-band shape reflecting its adolescent age. This subtle spectral peculiarity is shared by 1RXS J2351+3127 B and suggests a comparable age to LP 944-20 based on this morphology alone. (The 1.4–1.8 μm region of 1RXS J2351+3127 B, which samples the H_2O band depth and the entire H-band region, is also best-fit by the spectrum of LP 944-20.) However, since the spectral properties of brown dwarfs at intermediate ages are not well-calibrated, it is unclear how quickly these features evolve and therefore what robust age constraints can be obtained from this method.

Separate fits to individual bands produce best-fit spectral types of M9–L1.5. The 1.15–1.34 μm region yields the L0 (optical type: West et al. 2008)/M9 (NIR type: Kirkpatrick et al. 2010) object 2MASSJ 12490872+4157286. The best match to the 1.50–1.80 μm region is the L1.5 (NIR type: Kirkpatrick et al. 2010) object 2MASS J01472702+4731142. The 2.0–2.45 μm region ($\sim K$) is best fit by the L0 (optical type: Wilson et al. 2001) object HD 89744 B from Burgasser et al. (2008).[12] Finally, we note that the gravity-independent classification index from Allers et al. (2007) yields a spectral type of M$8.4^{+1.1}_{-1.0}$, which is consistent with our previous estimates.

3.4.2. *Moderate-Resolution SXD and OSIRIS Spectra*

In Figure 9 we compare our SXD spectrum to late-M and early-L dwarfs from the IRTF Spectral Library (Cushing et al. 2005). 1RXS J2351+3127 B most closely resembles the L0.5 and L1 field objects. A comparison of individual bands to the templates likewise suggests M9–L1. Like our prism spectrum, there is some contamination from the primary at shorter wavelengths, which results in a slightly bluer spectrum and artificially diminished line strengths. The H and K bands were less contaminated by the primary in the raw SXD data.

On the other hand, our OSIRIS spectrum was obtained with AO and the companion was well separated from the primary. The J-band spectrum is shown in Figure 10 relative to M8–L3 field templates. The best overall match is the L2 template, although L1–L3 objects are also good fits. The depth of the 1.25 μm K I gravity-sensitive lines (e.g., McGovern et al. 2004; Kirkpatrick et al. 2006; Allers et al. 2009) do not appear particularly shallow relative to the field objects, which excludes very young ages ($\lesssim$10 Myr). Recently Geißler et al. (2012) presented NIR spectroscopy of a new M8 ± 1 companion to the Pleiades member H II 1348. Their OSIRIS J-band spectrum also lacks shallow alkali lines, which suggests that any impact on these lines from low surface gravity occurs at younger ages, at least at this temperature. Altogether we adopt a spectral type of L0^{+2}_{-1} for 1RXS J2351+3127 B. The asymmetric error bars reflect the slightly earlier type suggested by the prism and SXD spectra compared to the OSIRIS spectrum.

3.5. *Physical Properties*

The mass of 1RXS J2351+3127 B can be estimated from its luminosity and age using substellar cooling models. Assuming a distance of 50 ± 10 pc, the K-band bolometric correction from Golimowski et al. (2004) yields a luminosity of $\log L/L_\odot = -3.6 \pm 0.2$ (the uncertainty incorporates intrinsic scatter in the relation, photometric errors, and a spectral type accuracy of one subtype).[13] The age estimate of the system depends on whether it is an AB Dor member, in which case the age of ∼50–150 Myr (see Section 4) can be leveraged from the entire cluster. If it is not a member then the constraints are much poorer, but probably lie between 50–500 Myr based on the high energy emission from the primary. We arrive at masses of 32 ± 6 $M_{\rm Jup}$ and 50 ± 11 $M_{\rm Jup}$ for age ranges of 50–150 Myr and 50–500 Myr, respectively, based on a grid of finely interpolated evolutionary models from Burrows et al. (1997).[14] Figure 11 shows the influence of the distance estimate on the inferred mass of 1RXS J2351+3127 B, which lies between ∼25–40 $M_{\rm Jup}$ for distances of 35–65 pc assuming an age of 50–150 Myr.

The mass of the primary can be obtained from stellar evolutionary models. 1RXS J2351+3127 A has a spectral type of M2.0 ± 0.5 which corresponds to an effective temperature of ∼3520 K (Drilling & Landolt 2000). At 100 Myr (500 Myr), the models of Baraffe et al. (1998) give a mass of 0.45 $M_\odot$ (0.40 $M_\odot$) for this temperature. Since the mass is only weakly dependent on age we adopt a value of 0.45 ± 0.05 $M_\odot$ for 1RXS J2351+3127 A. Note that we have made use of solar metallicity evolutionary models here (with Y=0.275 and $L_{\rm mix}$=H_P); a non-solar composition and any intrinsic errors in the evolutionary models will result in systematic errors in the inferred mass. We also compute the luminosity of the primary star using the H-band bolometric correction from Casagrande et al. (2008) and the system's photometric distance, which yields log $L/L_{\odot} = -1.37 \pm 0.19$.

---

[12] The primary star HD 89744 A (F7IV/V) was classified as a likely AB Dor member by López-Santiago et al. (2006) based on its space motion. However, it is also an exoplanet-host star and independent age estimates point to an older age of 1–3 Gyr, arguing against AB Dor membership (see Table 3, footnote i of Evans et al. 2011 for a summary). The X-ray luminosity based on the count rate and hardness ratio (HR1=–0.58) listed in the Second *ROSAT* PSPC Catalog is a modest 28.0 erg/s, which is comparable to field stars.

[13] Distances of {35, 45, 55, 65} ± 10 pc give $\log L/L_\odot$ ={–3.9±0.3, –3.6±0.2 ,–3.5±0.2, –3.3±0.1}.

[14] Quoted masses represent the medians and standard deviations of the resulting mass distributions assuming uniform input distributions for the luminosity and ages. Normally-distributed input values of –3.6 ± 0.2 dex and 100 ± 25 Myr (300 ±150 Myr) give a similar mass of 35 ± 7 $M_{\rm Jup}$ (56 ± 11 $M_{\rm Jup}$). We also compute masses using interpolated Lyon models from Chabrier et al. (2000, Dusty) and Baraffe et al. (2003, Cond), as well as Saumon & Marley (2008, both clear and cloudy versions). The resulting mass estimates are all consistent within a few $M_{\rm Jup}$, indicating that the dominant sources of error are the uncertainty in the age and distance rather than the choice of models.

4. DISCUSSION AND CONCLUSIONS

The AB Dor YMG was first recognized by Zuckerman et al. (2004) as a sparse but relatively nearby group of young stars in the Local Association with common space motions. Since its discovery there have been many attempts to identify additional members (López-Santiago et al. 2006; Torres et al. 2008; Zuckerman et al. 2011; McCarthy & White 2012), with recent attention mostly focused on filling in the lower main sequence (Shkolnik et al. 2009; Schlieder et al. 2010, 2012; Shkolnik et al. 2012). Age estimates for the cluster vary considerably. Studies of the AB Dor quadruple system itself have yielded values of ∼30–100 Myr using theoretical isochrones (Close et al. 2007; Janson et al. 2007; Boccaletti et al. 2008; Guirado et al. 2011). However, comparisons of AB Dor members to the Pleiades (∼125 Myr) and IC 2391 (35–50 Myr) clusters in color-magnitude diagrams by Luhman et al. (2005, see also Luhman & Potter 2006) make it clear that the AB Dor group is older than IC 2391 and approximately coeval with the Pleiades. Kinematic analysis of the cluster by Luhman et al. (2005) and Ortega et al. (2007) support a common origin and age with the Pleiades. In Figure 12 we compare the color-magnitude sequence of AB Dor members to Pleiades stars and brown dwarfs (see caption for details). The sequences line up well from the highest-mass B-type members down to the latest L dwarfs in both clusters, supporting the older Pleiades-like age of AB Dor.

A parallax for the 1RXS J2351+3127 AB system is needed to confirm its association with AB Dor. The large uncertainty in the photometric distance means the space motion of 1RXS J2351+3127 AB is only marginally constrained. At distances of 35–50 pc it agrees well with the kinematics of the AB Dor group, but it is inconsistent at larger distances given the relatively small internal velocity dispersion (a few km/s) of the moving group (Figure 7). If it does belong to the cluster then 1RXS J2351+3127 B is the second lowest-mass member of AB Dor after the L4 companion CD–35 2722 B (Wahhaj et al. 2011), which was recently discovered as part of the Gemini NICI Planet-Finding Campaign (Liu et al. 2010b). Note that 1RXS J2351+3127 B should have a distance $\gtrsim$45 pc for its position to be consistent with the later-type CD–35 2722 B in the color-magnitude diagram. This could be a clue that 1RXS J2351+3127 B is not in fact a member of AB Dor since distances larger than ∼50 pc produce space motions that differ from the cluster. As noted earlier, even if 1RXS J2351+3127 AB are not members, independent lines of evidence from the primary (high-energy emission) and the companion (*H*-band spectral morphology) indicate the system is young (∼100-500 Myr), and except for the oldest ages and the largest distances, the companion is substellar.

Already it is clear from the spectra of CD–35 2722 B obtained by Wahhaj et al. that L dwarfs at the age of the AB Dor moving group show few signs of youth. Like 1RXS J2351+3127 B, CD–35 2722 B has *J*-band absorption features comparable to field objects, and the shape of the *H* band is intermediate between the youngest brown dwarfs and old field objects. CD–35 2722 B has brighter absolute NIR magnitudes than field objects with the same spectral type so a parallax for 1RXS J2351+3127 B will also be useful to look for the same effect. One of the few studies to examine the near-infrared spectral properties of Pleiades brown dwarfs was carried out by Bihain et al. (2010). They obtained low-resolution spectra of M7–L3.5 Pleiades members and most exhibited shapes similar to field objects, with a few suggesting somewhat more angular *H*-band features with less 1.6 μm FeH absorption. These trends appear to be consistent with CD–35 2722 B and 1RXS J2351+3127 B.

A growing number of ultracool objects have been tied to the AB Dor YMG. In addition to 1RXS J2351+3127 B (L0) and CD–35 2722 B (L4), which also orbits an early-M dwarf, three isolated M7–M9 objects were recently found by Schlieder et al. (2012) to be likely AB Dor members, although parallaxes and radial velocities are needed for confirmation. Including the low-mass M6 star AB Dor C (Close et al. 2005), a sequence of AB Dor members spanning a range of temperatures and masses below the hydrogen-burning limit is beginning to emerge. Since the spectral morphology of brown dwarfs is sensitive to age, a detailed comparison of optical and near-infrared spectroscopy of AB Dor brown dwarfs to those in the Pleiades can eventually be used for relative age dating, perhaps with even greater precision than color-magnitude diagram comparisons.

We thank the referee for helpful comments, Joshua Schlieder for early access to his kinematic analysis of 1RXS J2351+3127 A, Katelyn Allers for helpful discussions about young brown dwarfs, Eric Nielsen for the background track predictions, and Carolin Liefke for providing us with the NEXXUS 2 catalog. It is a pleasure to thank the support astronomers and telescope operators at Keck and IRTF who helped make this work possible: Marc Kassis, Heather Hershley, Jim Lyke, Hien Tran, and John Rayner. BPB and MCL have been supported by NASA grant NNX11AC31G and NSF grant AST09-09222. ALK has been supported by NASA through Hubble Fellowship grant 51257.01 awarded by STScI, which is operated by AURA, INc., for NASA under contract NAS 5-26555. We utilized data products from the Two Micron All Sky Survey, which is a joint project of the University of Massachusetts and the Infrared Processing and Analysis Center/California Institute of Technology, funded by the National Aeronautics and Space Administration and the National Science Foundation. NASA's Astrophysics Data System Bibliographic Services together with the VizieR catalogue access tool and SIMBAD database operated at CDS, Strasbourg, France, were invaluable resources for this work. Finally, mahalo nui loa to the kamaʻāina of Hawaiʻi for their support of Keck and the Mauna Kea observatories. We are grateful to conduct observations from this mountain.

Facilities: Keck:II (NIRC2, OSIRIS), IRTF (SpeX)

REFERENCES

Allers, K. N., et al. 2007, ApJ, 657, 511
—. 2009, ApJ, 697, 824
Baraffe, I., Chabrier, G., Allard, F., & Hauschildt, P. H. 1998, A&A, 337, 403
Baraffe, I., Chabrier, G., Barman, T. S., Allard, F., & Hauschildt, P. H. 2003, A&A, 402, 701
Barman, T. S., Macintosh, B., Konopacky, Q. M., & Marois, C. 2011, ApJ, 733, 65
Barnes, S. A., & Kim, Y.-C. 2010, ApJ, 721, 675
Barrado, D. 1998, A&A, 339, 831
Berger, E., et al. 2001, Nature, 410, 338
Bergfors, C., et al. 2010, A&A, 520, A54
Beuzit, J.-L., et al. 2008, 7014, 701418
Bihain, G., Rebolo, R., Béjar, V. J. S., Caballero, J. A., Bailer-Jones, C. A. L., Mundt, R., Acosta-Pulido, J. A., & Torres, A. M. 2006, A&A, 458, 805
Bihain, G., Rebolo, R., Osorio, M. R. Z., Béjar, V. J. S., & Caballero, J. A. 2010, A&A, 519, A93
Biller, B. A., et al. 2007, ApJSS, 173, 143
Boccaletti, A., Chauvin, G., Baudoz, P., & Beuzit, J.-L. 2008, A&A, 482, 939
Bonfils, X., et al. 2011, arXiv:astro-ph/1111.5019
Bowler, B. P., Liu, M. C., Dupuy, T. J., & Cushing, M. C. 2010, ApJ, 723, 850
Burgasser, A. J., Liu, M. C., Ireland, M. J., Cruz, K. L., & Dupuy, T. J. 2008, ApJ, 681, 579
Burgasser, A. J., & McElwain, M. W. 2006, AJ, 131, 1007
Burrows, A., et al. 1997, ApJ, 491, 856
Casagrande, L., Flynn, C., & Bessell, M. 2008, MNRAS, 389, 585
Cassan, A., et al. 2012, Nature, 481, 167
Chabrier, G., Baraffe, I., Allard, F., & Hauschildt, P. 2000, ApJ, 542, 464
Chauvin, G., et al. 2010, A&A, 509, A52
Close, L. M., et al. 2005, Nature, 433, 286
Close, L. M., Thatte, N., Nielsen, E. L., Abuter, R., Clarke, F., & Tecza, M. 2007, ApJ, 665, 736
Crepp, J. R., et al. 2011, arXiv/astro-ph: 1112.1725, astro-ph.EP
Cushing, M. C., Rayner, J. T., & Vacca, W. D. 2005, ApJ, 623, 1115
Cushing, M. C., Vacca, W. D., & Rayner, J. T. 2004, PASP, 116, 362
Delfosse, X., Forveille, T., Perrier, C., & Mayor, M. 1998, A&A, 331, 581
Drilling, J. S., & Landolt, A. U. 2000, in Allen's Astrophysical Quantities, 4th ed., ed. A. N. Cox (New York, NY: AIP Press; Springer 2000), 381
Dupuy, T. J., & Liu, M. C. 2012, arXiv/astro-ph:1201.2465v1
Dupuy, T. J., Liu, M. C., & Ireland, M. J. 2009, ApJ, 692, 729
Duquennoy, A., & Mayor, M. 1991, A&A, 248, 485
Endl, M., Cochran, W. D., Kürster, M., Paulson, D. B., Wittenmyer, R. A., MacQueen, P. J., & Tull, R. G. 2006, ApJ, 649, 436
Evans, T. M., et al. 2011, ApJ, 744, 120
Feigelson, E. D., et al. 2004, ApJ, 611, 1107
Feigelson, E. D., & Montmerle, T. 1999, Annu. Rev. Astro. Astrophys., 37, 363
Findeisen, K., Hillenbrand, L., & Soderblom, D. 2011, AJ, 142, 23
Fischer, D. A., & Marcy, G. W. 1992, ApJ, 396, 178
Fleming, T. A., Molendi, S., Maccacaro, T., & Wolter, A. 1995, Astrophysical Journal Supplement v.99, 99, 701
Galli, P. A. B., Teixeira, R., Ducourant, C., Bertout, C., & Benevides-Soares, P. 2012, Astronomy & Astrophysics, 538, A23
Geißler, K., Metchev, S. A., Pham, A., Larkin, J. E., McElwain, M., & Hillenbrand, L. A. 2012, ApJ, 746, 44
Golimowski, D. A., et al. 2004, AJ, 127, 3516
Gould, A., et al. 2010, ApJ, 720, 1073
—. 2006, ApJ, 644, L37
Green, D. A. 2011, Bulletin of the Astromical Society of India, 39, 289
Guirado, J. C., Marcaide, J. M., Martí-Vidal, I., Bouquin, J.-B. L., Close, L. M., Cotton, W. D., & Montalbán, J. 2011, Astronomy & Astrophysics, 533, A106
Henry, T. J. 2004, In Spectroscopically and Spatially Resolving the Components of the Close Binary Stars, 318, 159
Henry, T. J., Ianna, P. A., Kirkpatrick, J. D., & Jahreiss, H. 1997, Astron. J. 114, 114, 388
Hillenbrand, L. A., Foster, J. B., Persson, S. E., & Matthews, K. 2002, PASP, 114, 708
Hinkley, S., et al. 2011, PASP, 123, 74
Irwin, J., Berta, Z. K., Burke, C. J., Charbonneau, D., Nutzman, P., West, A. A., & Falco, E. E. 2011, ApJ, 727, 56
Janson, M., Brandner, W., Lenzen, R., Close, L., Nielsen, E., Hartung, M., Henning, T., & Bouy, H. 2007, A&A, 462, 615
Johnson, J. A., Aller, K. M., Howard, A. W., & Crepp, J. R. 2010, PASP, 122, 905
Johnson, J. A., & Apps, K. 2009, ApJ, 699, 933
Johnson, J. A., Butler, R. P., Marcy, G. W., Fischer, D. A., Vogt, S. S., Wright, J. T., & Peek, K. M. G. 2007, ApJ, 670, 833
Kastner, J. H., Crigger, L., Rich, M., & Weintraub, D. A. 2003, ApJ, 585, 878
Kennedy, G. M., & Kenyon, S. J. 2008, ApJ, 673, 502
Kirkpatrick, J. D., Barman, T. S., Burgasser, A. J., McGovern, M. R., McLean, I. S., Tinney, C. G., & Lowrance, P. J. 2006, ApJ, 639, 1120
Kirkpatrick, J. D., et al. 2010, ApJS, 190, 100
Kraus, A. L., Ireland, M. J., Hillenbrand, L. A., & Martinache, F. 2012, ApJ, 745, 19
Lada, C. J. 2006, ApJ, 640, L63
Lafrenière, D., et al. 2007, ApJ, 670, 1367
Larkin, J., et al. 2006, New Astronomy Reviews, 50, 362
Leggett, S. K., et al. 2006, MNRAS, 373, 781
Lépine, S., & Simon, M. 2009, AJ, 137, 3632
Liu, M. C. 2004, Science, 305, 1442
Liu, M. C., Dupuy, T. J., & Leggett, S. K. 2010a, ApJ, 722, 311
Liu, M. C., Fischer, D. A., Graham, J. R., Lloyd, J. P., Marcy, G. W., & Butler, R. P. 2002, ApJ, 571, 519
Liu, M. C., et al. 2010b, Adaptive Optics Systems II. Edited by Ellerbroek, 7736, 53
Lodieu, N., Hambly, N. C., Jameson, R. F., & Hodgkin, S. T. 2008, MNRAS, 383, 1385
Looper, D. L., Burgasser, A. J., Kirkpatrick, J. D., & Swift, B. J. 2007, ApJ, 669, L97
López-Santiago, J., Montes, D., Crespo-Chacón, I., & Fernández-Figueroa, M. J. 2006, ApJ, 643, 1160
Lucas, P. W., Roche, P. F., Allard, F., & Hauschildt, P. H. 2001, MNRAS, 326, 695
Luhman, K. L., et al. 2007, ApJ, 654, 570
Luhman, K. L., & Potter, D. 2006, ApJ, 638, 887
Luhman, K. L., Stauffer, J. R., & Mamajek, E. E. 2005, ApJ, 628, L69
Lupton, R., Blanton, M. R., Fekete, G., Hogg, D. W., O'Mullane, W., Szalay, A., & Wherry, N. 2004, PASP, 116, 133
Macintosh, B., et al. 2006, Advances in Adaptive Optics II. Edited by Ellerbroek, 6272, 18
Mamajek, E. E. 2005, ApJ, 634, 1385
Marois, C., Lafrenière, D., Doyon, R., Macintosh, B., & Nadeau, D. 2006, ApJ, 641, 556
Martin, D. C., et al. 2005, ApJ, 619, L1
Martín, E. L., Guenther, E., Osorio, M. R. Z., Bouy, H., & Wainscoat, R. 2006, ApJ, 644, L75
Martinache, F., & Guyon, O. 2009, Techniques and Instrumentation for Detection of Exoplanets IV. Edited by Shaklan, 7440, 20
McCarthy, K. A., & White, R. J. 2012, arXiv/astro-ph:1201.6600
McGovern, M. R., Kirkpatrick, J. D., McLean, I. S., Burgasser, A. J., Prato, L., & Lowrance, P. J. 2004, ApJ, 600, 1020
Morrissey, P., et al. 2007, ApJSS, 173, 682
Neuhäuser, R., Sterzik, M. F., Schmitt, J. H. M. M., Wichmann, R., & Krautter, J. 1995, A&A, 297, 391
Nielsen, E. L., & Close, L. M. 2010, ApJ, 717, 878
Nielsen, E. L., Close, L. M., Biller, B. A., Masciadri, E., & Lenzen, R. 2008, ApJ, 674, 466
Ortega, V. G., Jilinski, E., Reza, R. D. L., & Bazzanella, B. 2007, MNRAS, 377, 441
Pagano, I. 2009, Astrophysics and Space Science, 320, 115
Pavlenko, Y. V., Jones, H. R. A., Martín, E. L., Guenther, E., Kenworthy, M. A., & Osorio, M. R. Z. 2007, MNRAS, 380, 1285
Pizzolato, N., Maggio, A., Micela, G., Sciortino, S., & Ventura, P. 2003, A&A, 397, 147

Preibisch, T., Balega, Y., Hofmann, K.-H., Weigelt, G., & Zinnecker, H. 1999, New Astronomy, 4, 531

Preibisch, T., & Feigelson, E. D. 2005, ApJSS, 160, 390

Preibisch, T., & Mamajek, E. 2008, Handbook of Star Forming Regions, 235

Raghavan, D., et al. 2010, ApJSS, 190, 1

Rayner, J. T., Toomey, D. W., Onaka, P. M., Denault, A. J., Stahlberger, W. E., Vacca, W. D., Cushing, M. C., & Wang, S. 2003, PASP, 115, 362

Reid, I. N., Cruz, K. L., & Allen, P. R. 2007, AJ, 133, 2825

Reiners, A., & Mohanty, S. 2012, ApJ, 746, 43

Riaz, B., Gizis, J. E., & Harvin, J. 2006, AJ, 132, 866

Ribas, I. 2003, A&A, 400, 297

Ribas, I., Guinan, E. F., Güdel, M., & Audard, M. 2005, ApJ, 622, 680

Rice, E. L., Faherty, J. K., & Cruz, K. L. 2010, ApJ, 715, L165

Robinson, R. D., et al. 2005, ApJ, 633, 447

Rodriguez, D. R., Bessell, M. S., Zuckerman, B., & Kastner, J. H. 2011, ApJ, 727, 62

Rojas-Ayala, B., Covey, K. R., Muirhead, P. S., & Lloyd, J. P. 2010, ApJ, 720, L113

Rutledge, R. E., Basri, G., Martín, E. L., & Bildsten, L. 2000, ApJ, 538, L141

Saumon, D., & Marley, M. S. 2008, ApJ, 689, 1327

Schlieder, J. E., Lépine, S., & Simon, M. 2010, AJ, 140, 119

—. 2012, AJ, 143, 80

Schmitt, J. H. M. M., & Liefke, C. 2004, A&A, 417, 651

Shkolnik, E., Liu, M. C., & Reid, I. N. 2009, ApJ, 699, 649

Shkolnik, E. L., Liu, M. C., Reid, I. N., Dupuy, T., & Weinberger, A. J. 2011, ApJ, 727, 6

Simon, T., Herbig, G., & Boesgaard, A. M. 1985, ApJ, 293, 551

Simons, D. A., & Tokunaga, A. 2002, PASP, 114, 169

Skrutskie, M. F., et al. 2006, AJ, 131, 1163

Skumanich, A. 1972, ApJ, 171, 565

Soderblom, D. R., Nelan, E., Benedict, G. F., McArthur, B., Ramirez, I., Spiesman, W., & Jones, B. F. 2005, AJ, 129, 1616

Stauffer, J. R., et al. 2007, ApJSS, 172, 663

Sumi, T., et al. 2010, ApJ, 710, 1641

—. 2011, Nature, 473, 349

Terrien, R. C., Mahadevan, S., Bender, C. F., Deshpande, R., Ramsey, L. W., & Bochanski, J. J. 2012, ApJ, 747, L38

Tinney, C. G. 1998, MNRAS, 296, L42

Tinney, C. G., & Tolley, A. J. 1999, MNRAS, 304, 119

Tokunaga, A. T. 2000, in Allen's Astrophysical Quantities, 4th ed., ed. A. N. Cox (New York, NY: AIP Press; Springer 2000), 143

Tokunaga, A. T., & Vacca, W. D. 2005, PASP, 117, 421

Torres, C. A. O., Quast, G. R., da Silva, L., Reza, R. D. L., Melo, C. H. F., & Sterzik, M. 2006, A&A, 460, 695

Torres, C. A. O., Quast, G. R., Melo, C. H. F., & Sterzik, M. F. 2008, Handbook of Star Forming Regions, 757

Torres, G., & Ribas, I. 2002, ApJ, 567, 1140

Vacca, W. D., Cushing, M. C., & Rayner, J. T. 2003, PASP, 115, 389

Voges, W., et al. 1999, A&A, 349, 389

Wahhaj, Z., et al. 2011, ApJ, 729, 139

West, A. A., Hawley, S. L., Bochanski, J. J., Covey, K. R., Reid, I. N., Dhital, S., Hilton, E. J., & Masuda, M. 2008, AJ, 135, 785

Wilson, J. C., Kirkpatrick, J. D., Gizis, J. E., Skrutskie, M. F., Monet, D. G., & Houck, J. R. 2001, AJ, 122, 1989

Wizinowich, P., et al. 2000, PASP, 112, 315

Wright, N. J., Drake, J. J., Mamajek, E. E., & Henry, G. W. 2011, ApJ, 743, 48

Yelda, S., Lu, J. R., Ghez, A. M., Clarkson, W., Anderson, J., Do, T., & Matthews, K. 2010, ApJ, 725, 331

Zacharias, N., et al. 2010, AJ, 139, 2184

Zuckerman, B., Rhee, J. H., Song, I., & Bessell, M. S. 2011, ApJ, 732, 61

Zuckerman, B., Song, I., & Bessell, M. S. 2004, ApJ, 613, L65

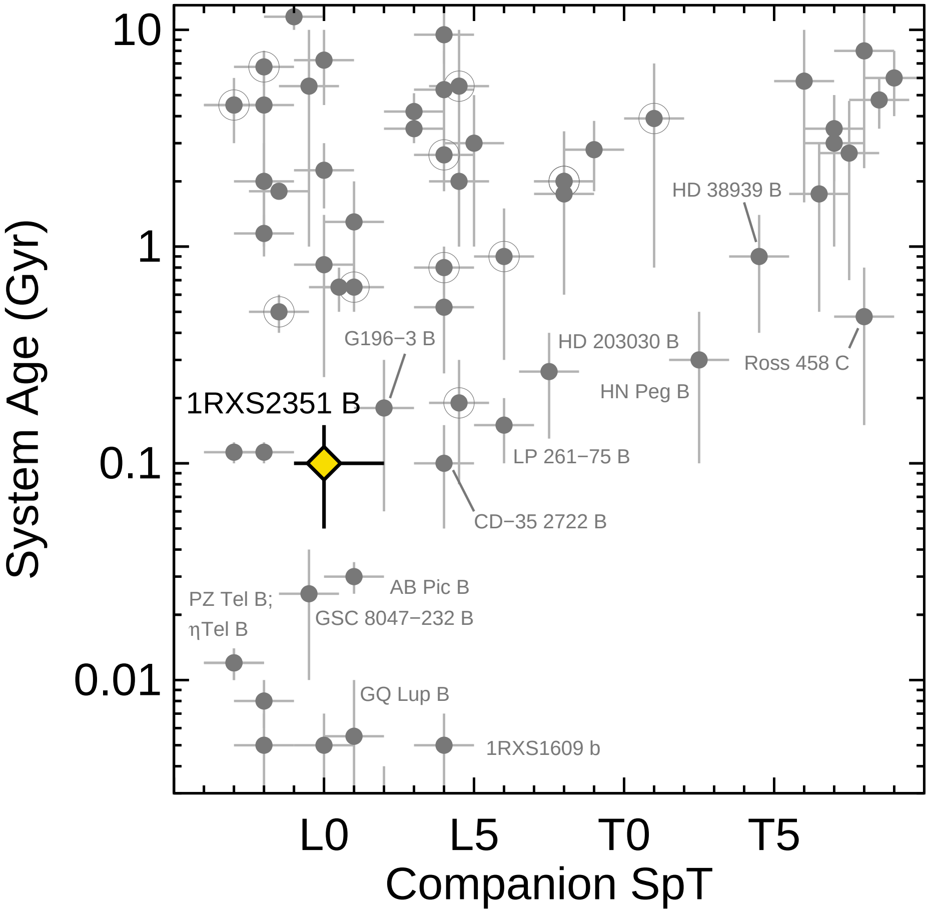

Fig. 1.— Census of benchmark ultracool companions compiled from the literature. The sample is limited to main-sequence primaries with spectral types earlier than M5 and systems with well-constrained ages. Companions resolved into tight binaries are indicated with open circles and some of the younger/more recent discoveries are labeled. The HR 8799 planets are excluded because of their peculiar spectral and photometric properties (e.g., Bowler et al. 2010; Barman et al. 2011). In addition to 1RXS J2351+3127 AB only a handful other systems with ages of ∼50-300 Myr are known. A number of interesting features are apparent from this figure. There is a dearth of mid-L to T dwarf companions at young ages ($\lesssim$200 Myr), which corresponds to objects near and below the deuterium-burning limit. At old ages ($\gtrsim$7 Gyr) no late-L or early-T dwarf companions are known. While this could be a selection effect, it may also be showing the luminosity/temperature gap differentiating the lowest-mass stars, which have nearly constant temperatures at old ages, from brown dwarfs, which cool over time. Note that the compilation is incomplete for late-M dwarfs, especially at old ages.

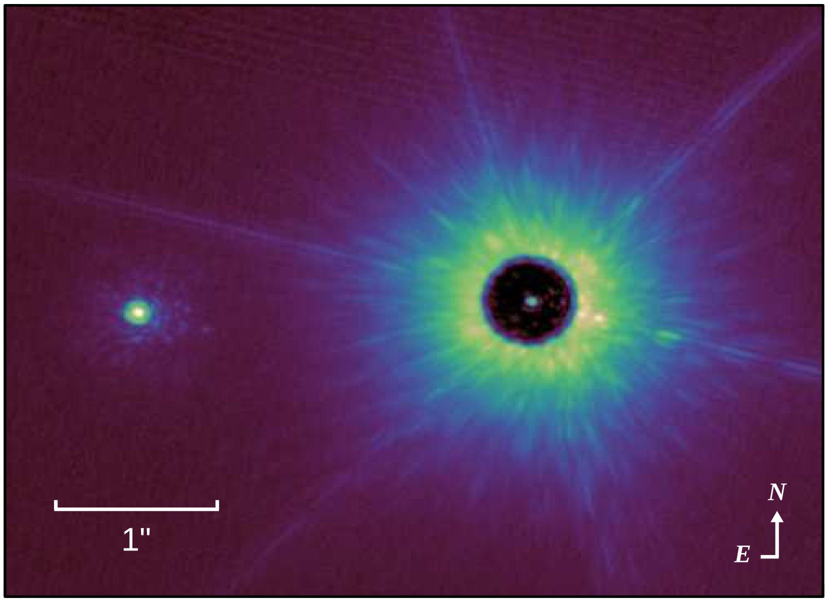

Fig. 2.— Keck/NIRC2 coadded H-band image of 1RXS J2351+3127 AB. The primary is positioned behind the $0\farcs6$ diameter translucent coronagraph with the companion located to its east. Both objects appear to be single down to the diffraction limit of Keck (∼40 mas). The image is displayed with an asinh stretch (Lupton et al. 2004) and the "cubehelix" color scheme of Green (2011).

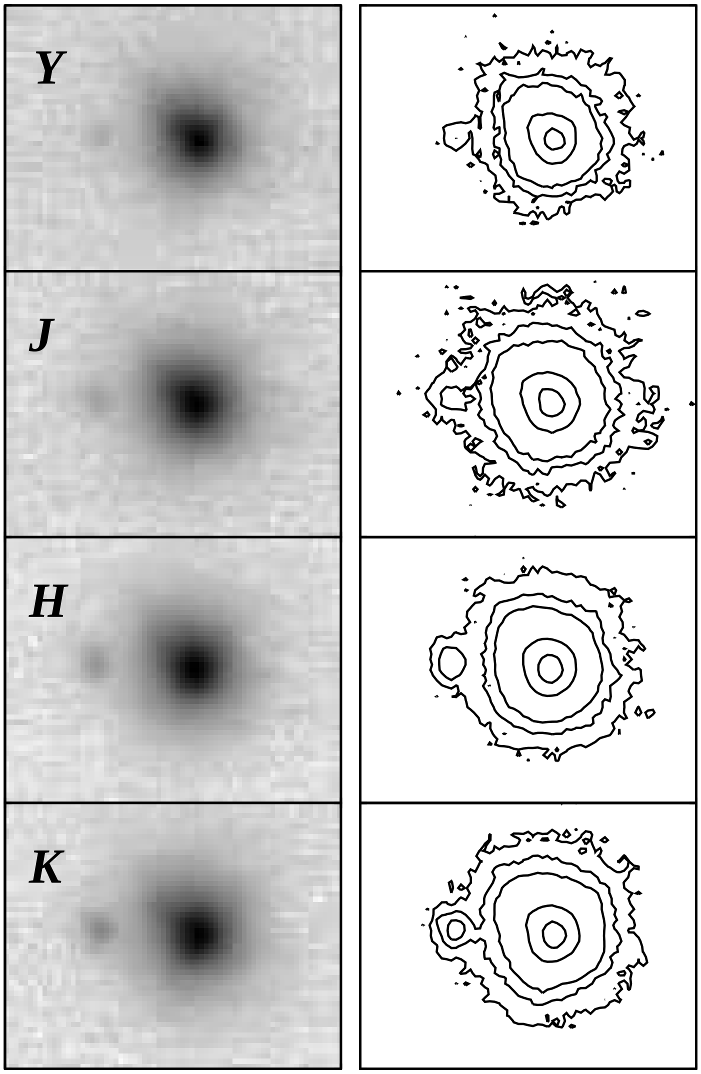

FIG. 3.— IRTF/SpeX guider camera $YJHK$ images of 1RXS J2351+3127 AB. The panels on the left show the stacked images of the system depicted with an asinh stretch. The panels on the right show contours representing 50%, 10%, 1%, 0.5%, and 0.2% of the peak flux from the primary.

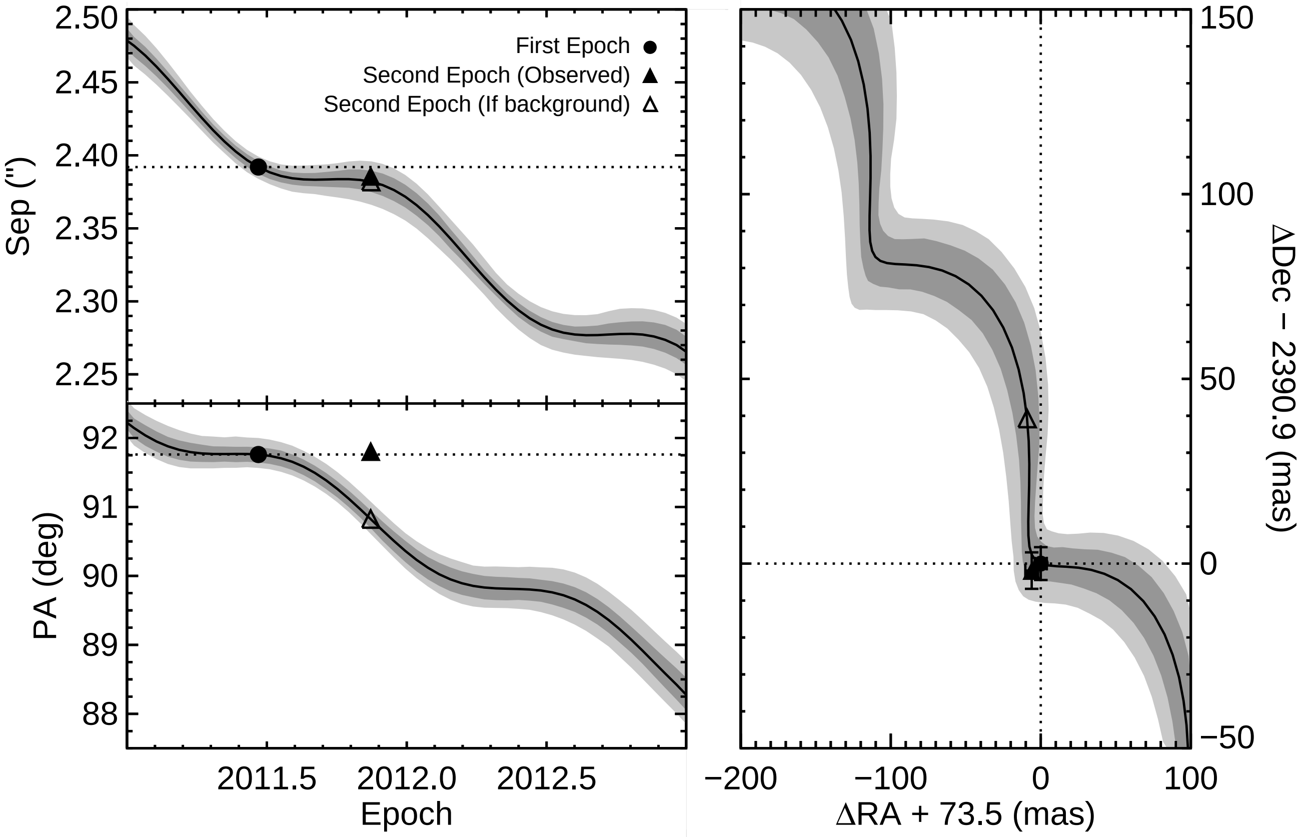

Fig. 4.— Astrometry for 1RXS J2351+3127 AB. *Left*: Separation (top) and position angle (bottom) of the companion at two epochs in 2011. The solid line shows the expected astrometry of a distant background object at the location of the companion in the first epoch data as a result of proper and parallax motion of the primary. The gray shaded regions represent 1- and 2-σ errors in the background tracks based on uncertainties in the proper motion, distance, and first epoch astrometry (solid circle). The second epoch astrometry (solid triangle) is inconsistent with the expected position (in PA but not separation) if it were a background object (open triangle). The astrometric uncertainties are smaller than the size of the symbols. *Right*: Same as the left panel except for ΔRA and ΔDec as seen on the sky (Δ refers to primary – secondary position). There is essentially no change in RA and Dec between the two epochs.

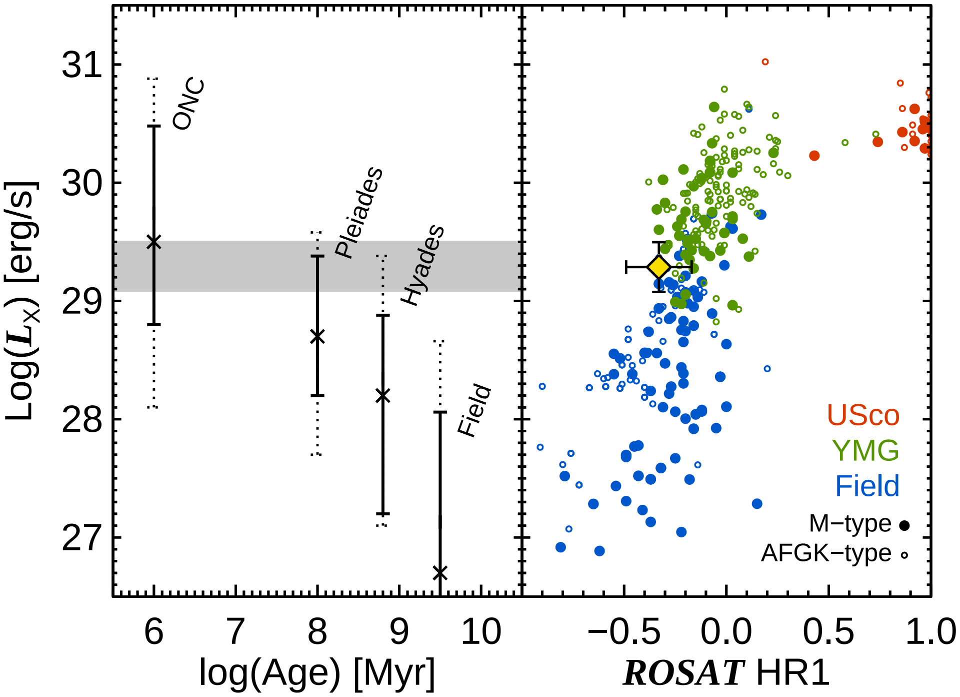

Fig. 5.— *Left*: Distributions of X-ray luminosities for low-mas stars (0.1–0.5 $M_\odot$) as a function of age from Preibisch & Feigelson (2005). Solid and dashed lines represent 68.3% and 95.4% ranges about the median for each distribution, respectively. Note that Preibisch & Feigelson (2005) applied a conversion factor to compare the X-ray luminosities from *ROSAT* for the Pleiades, Hyades, and field populations to the results for the ONC from *Chandra*. We converted these values back into *ROSAT* bandpasses and did the same for the ONC data. The X-ray luminosity of 1RXS J2351+3127 A is higher than the low-mass field population and most Hyades members. *Right*: X-ray luminosity vs. *ROSAT* hardness ratio 1 for USco members (red; Preibisch & Mamajek 2008), YMG members (green; Torres et al. 2008), and field stars (blue; Schmitt & Liefke 2004). M-type stars are plotted as filled circles and AFGK-type stars are shown with smaller open circles. Young stars have high X-ray luminosities and hardness ratios near zero, although we note that non-detections are not taken into account here. 1RXS J2351+3127 A is consistent with ∼10-100 Myr YMG members assuming a photometric distance of 50 ±10 pc.

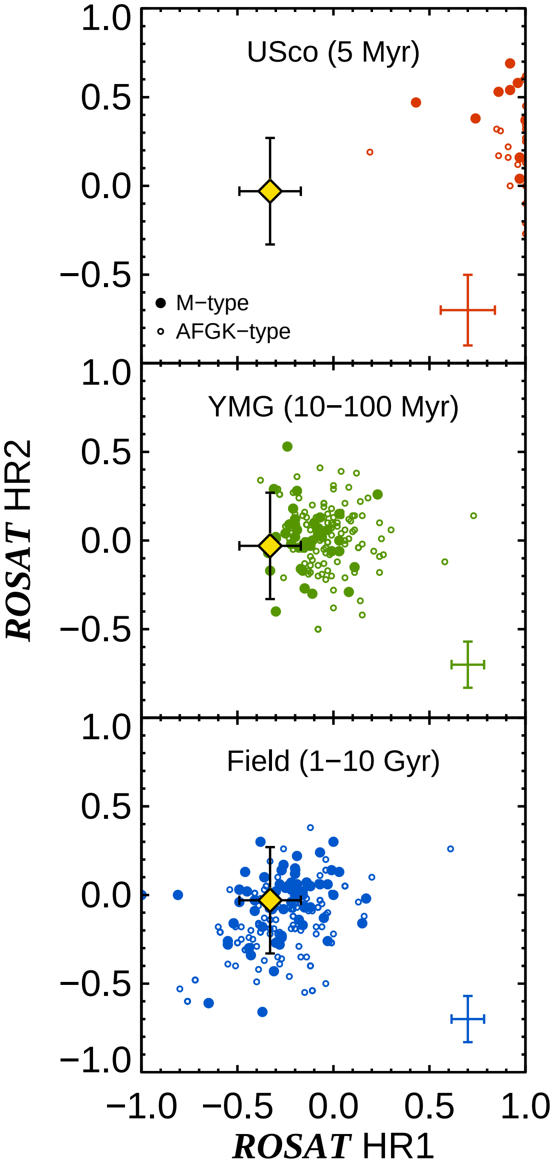

Fig. 6.— *ROSAT* PSPC hardness ratios for members of Upper Scorpius (top; Preibisch & Mamajek 2008), YMG members (middle; Torres et al. 2008), and field stars within 15 pc (bottom; NEXXUS 2 catalog: Schmitt & Liefke 2004). M-type stars are plotted as filled circles and AFGK-type stars are shown with smaller open circles. Hardness ratios soften over time (Kastner et al. 2003) and can be used as a rough proxy for age. 1RXS J2351+3127 A is consistent with YMG members and field objects. Typical uncertainties are shown in the bottom right of each panel.

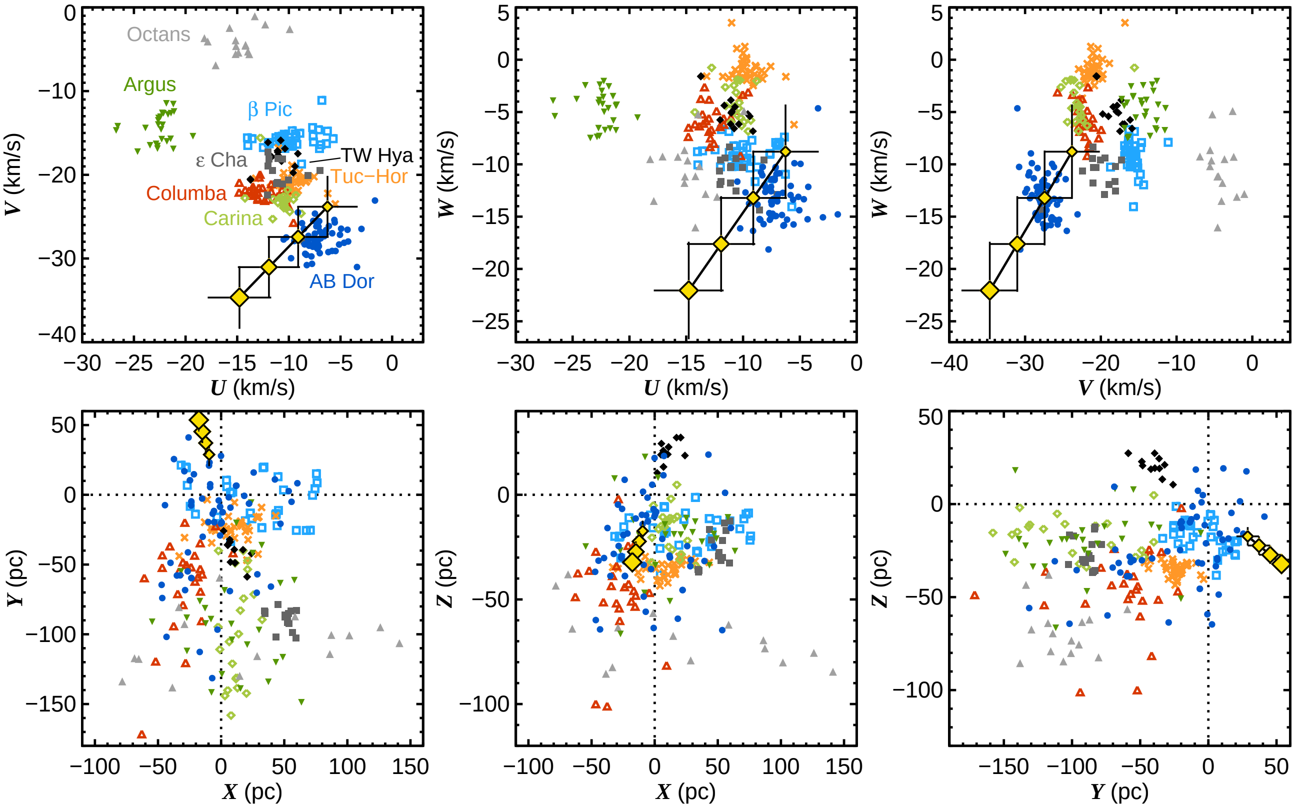

Fig. 7.— Space motion and relative positions of nearby YMGs from Torres et al. (2008). Distances (both measured parallaxes and kinematic estimates) are from Torres et al., while radial velocities are compiled from Simbad. The Octans (filled triangles), Argus (filled down-facing triangles), β Pic (open squares), ϵ Cha (filled squares), TW Hya (filled diamonds), Tuc-Hor (crosses), Columba (open triangles), Carina (open diamonds), and AB Dor (filled circles) groups occupy unique loci in UVW space. 1RXS J2351+3127 AB is overplotted as a series of increasingly-larger yellow diamonds which represent distances of 35, 45, 55, and 65 pc. The system's photometric distance of 50 pc coincides well with the AB Dor YMG, but distances larger than ~55 pc disagree with the kinematics of known members. Error bars include uncertainties in the distance estimate (10 pc), proper motion, and radial velocity. The AB Dor YMG is physically dispersed over a large region of sky; 1RXS J2351+3127 AB is consistent with the cluster in XYZ space, albeit near the border of where known members lie.

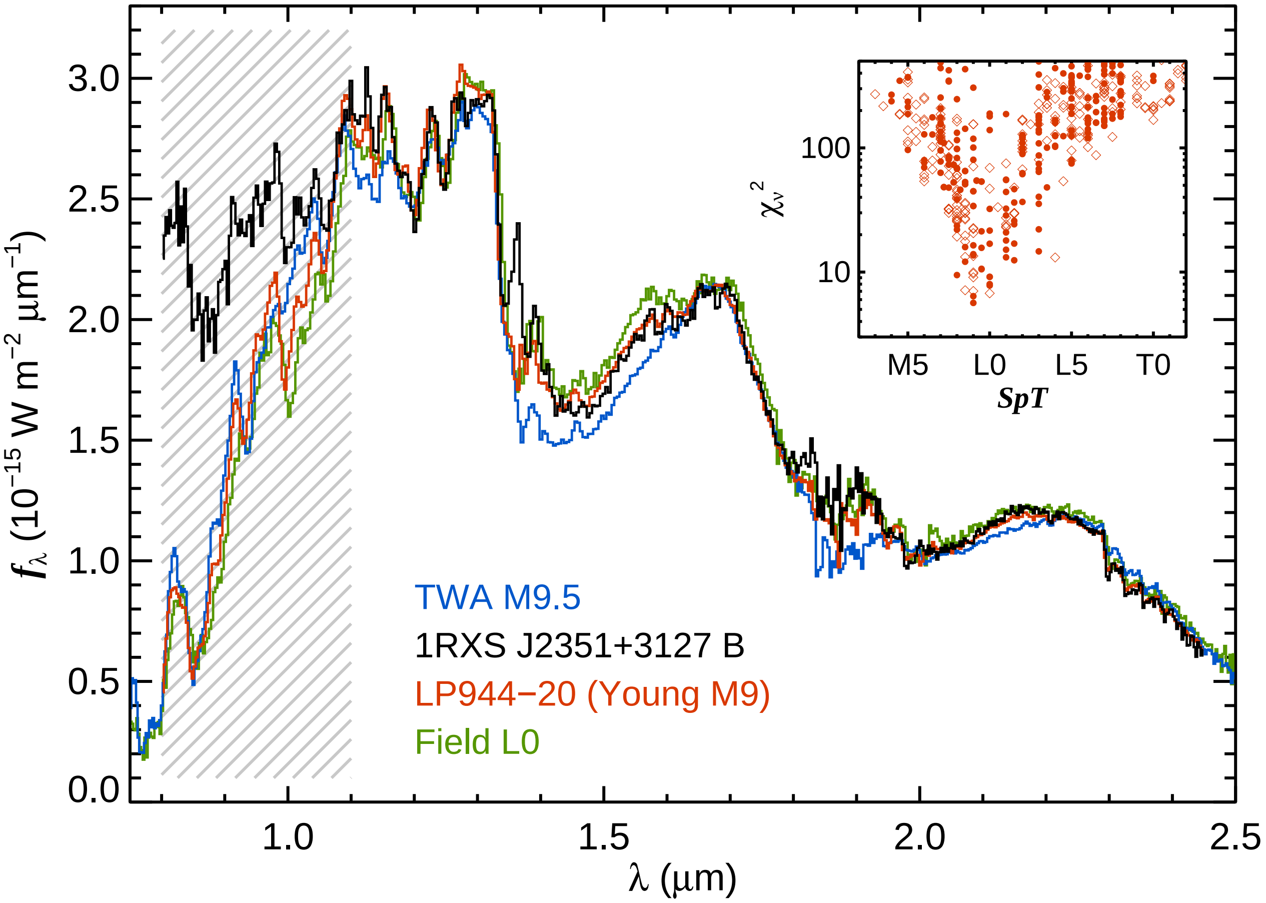

FIG. 8.— IRTF/SpeX prism spectrum of 1RXS J2351+3127 B (black). The 1.15–2.45 μm region is best matched by the ∼200–400 Myr M9 brown dwarf LP 944-20 (red). Contamination from the primary is evident at wavelengths shorter than ∼1.1 μm and is shown with gray shading. The L0 optical standard 2MASS J0345432+254023 (green) and the young (∼10 Myr) M9.5 TWA member 2MASS J11395113–3159214 (blue) are shown for comparison. The *H*-band region of 1RXS J2351+3127 B and LP 944-20 appear intermediate between the old field object and the young brown dwarf, although the effect is subtle. Note that LP 944-20 is scaled to 1RXS J2351+3127 B by minimizing the χ^2 value, while the field and young objects are normalized to the 1.68–1.70 μm region. The inset shows the reduced χ^2 values of fits to MLT dwarfs from the SpeX Prism Library plotted against spectral type. When optical types (filled circles) are not available we use near-infrared types (open diamonds).

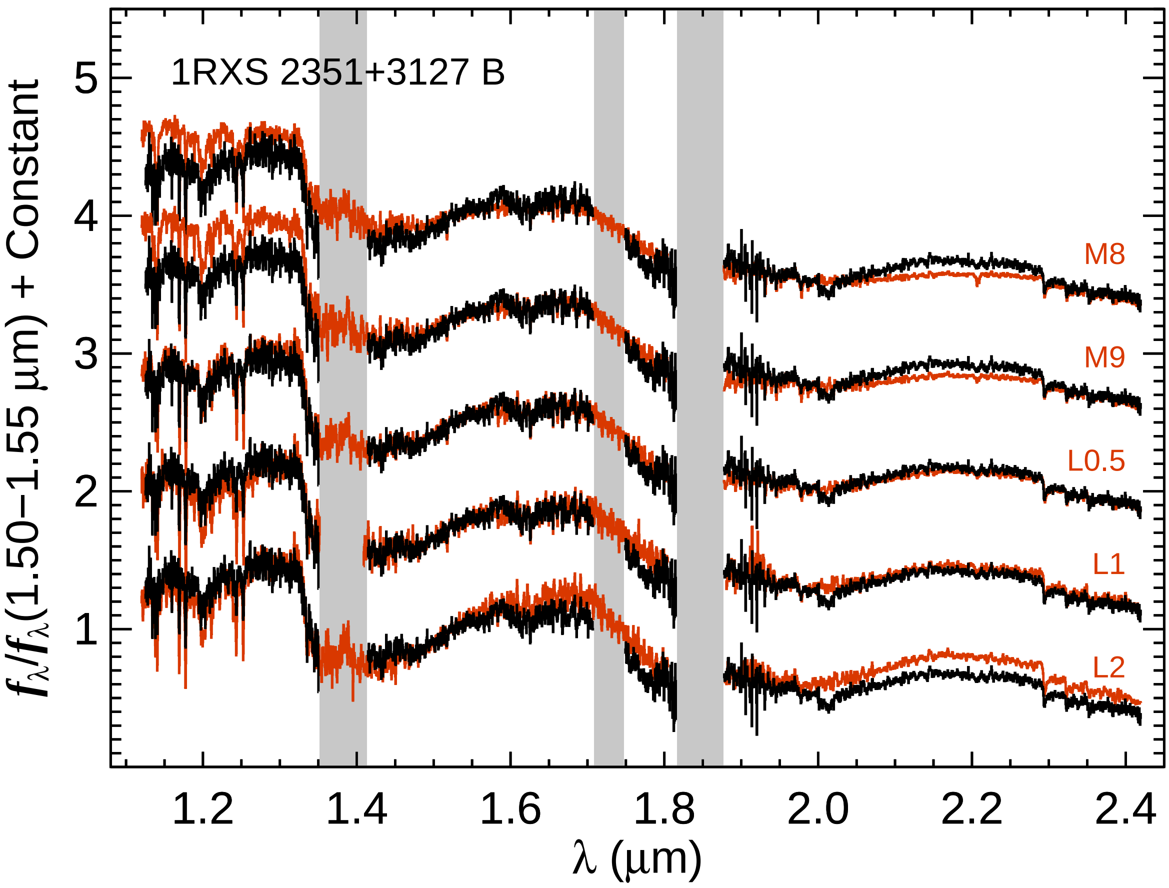

Fig. 9.— IRTF/SpeX SXD spectrum of 1RXS J2351+3127 B compared to field M and L dwarfs from the IRTF Spectral Library (Cushing et al. 2005). The L0.5 and L1 templates are close matches to 1RXS J2351+3127 B. The spectra are normalized beetwen 1.50-1.55 μm and offset by a constant. Gaps in the spectrum of 1RXS J2351+3127 B are caused by strong telluric absorption between 1.35–1.40 μm, a ghost feature between 1.71–1.75 μm caused by the placement on the detector, and a gap between orders from 1.82–1.87 μm.

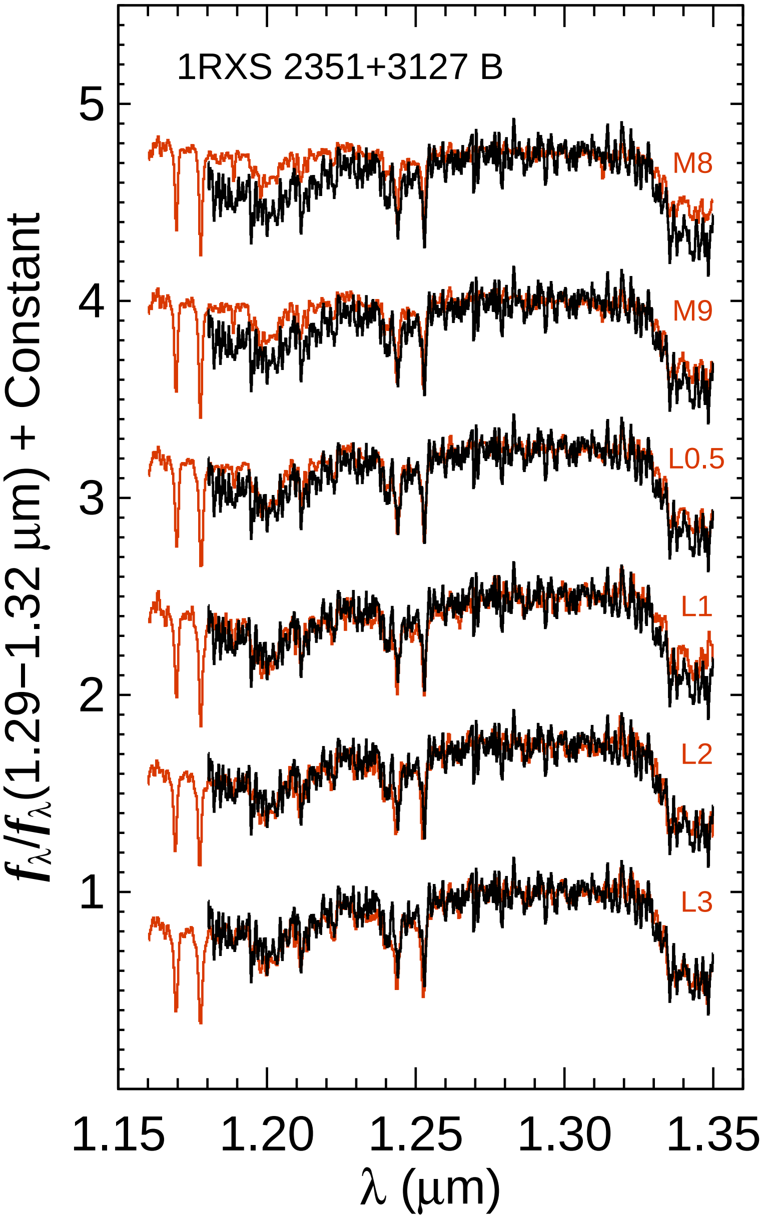

Fig. 10.— Keck-II/OSIRIS *J*-band spectrum of 1RXS J2351+3127 B compared to field objects from the IRTF Spectral Library. The depth of the 1.244/1.253 μm K I lines are comparable to field objects, implying 1RXS J2351+3127 B is not exceptionally young ($\lesssim$10 Myr). The best matches are L1–L3 spectral types.

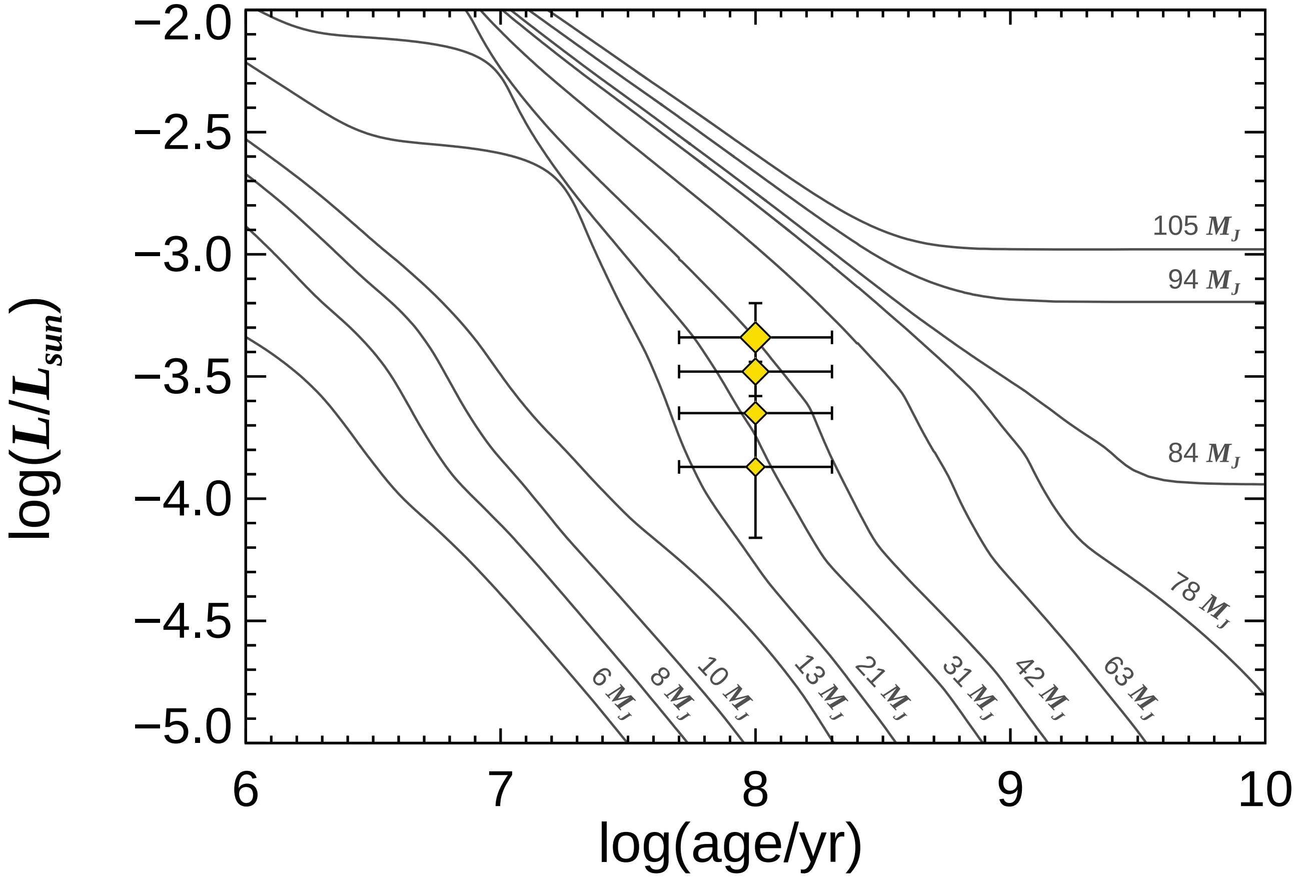

Fig. 11.— The mass of 1RXS J2351+3127 B based on the substellar evolutionary models of Burrows et al. (1997). Yellow diamonds show the luminosity of 1RXS J2351+3127 B for distances of 35, 45, 55, and 65 pc with increasing size indicating larger distance. If 1RXS J2351+3127 AB is a member of the AB Dor moving group (∼50–150 Myr), its photometric distance (50 ± 10 pc) implies a mass of 32 ± 6 $M_{\rm Jup}$ for the companion. If the system is not a member and the age range is ∼50-500 Myr, the mass estimate increases to 50 ± 11 $M_{\rm Jup}$.

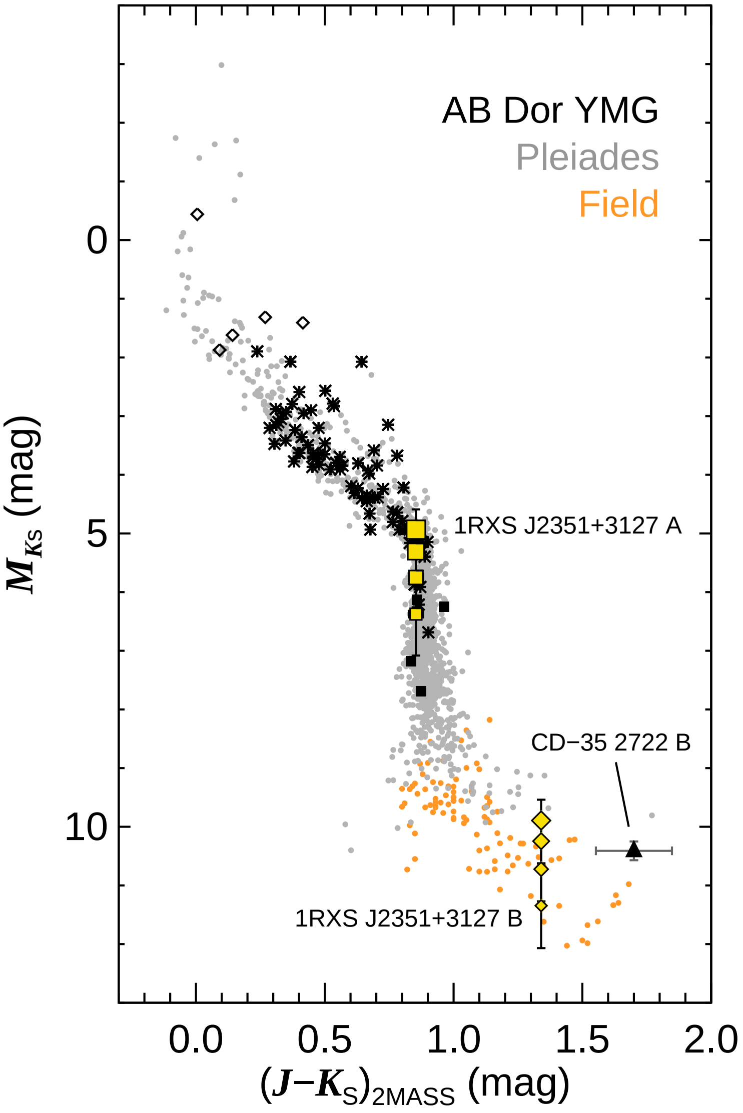

FIG. 12.— Color-magnitude diagram for the AB Dor moving group. The sequence of Pleiades members from Stauffer et al. (2007) and Bihain et al. (2010) are shown in gray, and field ultracool dwarfs from Dupuy & Liu (2012) are plotted in orange. The AB Dor members are compiled from Torres et al. (2008, stars), Zuckerman et al. (2011, open diamonds), and Shkolnik et al. (2012, submitted; filled squares). Except for the Torres et al. list, only objects with parallaxes and good 2MASS photometry are plotted. The AB Dor sequence appears to be indistinguishable from the Pleiades sequence, at least in J-K. The positions of 1RXS J2351+3127 AB are plotted with yellow squares (primary) and diamonds (companion) for distances of 35–65 pc. The filled triangle shows CD–35 2722 B (Wahhaj et al. 2011, L4 ± 1), which is the latest-type member of AB Dor currently known. Its photometry was converted from the MKO to 2MASS systems using the relations from Leggett et al. (2006). Note that AB Dor C (M6 ± 1) is not displayed because of the large uncertainties in its near-infrared colors (Luhman & Potter 2006).

TABLE 1
Summary of Observations

UT Date (Y/M/D)	Target (A/B)	Instrument	Filter/$\lambda\lambda$	No. of Exposures	Coadds × Exp. Time (s)
			Imaging		
2011/06/21	A	Keck-II/NIRC2	H	5	100×0.028
2011/06/21	A+B	Keck-II/NIRC2	H	5	1×10
2011/11/15	A+B	Keck-II/NIRC2	K'	9	50×0.2
2011/12/02	A+B	IRTF/SpeX	Y	8	2×10
2011/12/02	A+B	IRTF/SpeX	J	20	5×1.5
2011/12/02	A+B	IRTF/SpeX	H	20	10×1
2011/12/02	A+B	IRTF/SpeX	K	20	2×2
			Spectroscopy		
2011/10/14	B	IRTF/SpeX-prism	0.8–2.5 μm	6	1×120
2011/12/02	A+B	IRTF/SpeX-SXD	1.1–2.5 μm	24	1×120
2011/12/26	B	Keck-II/OSIRIS	1.18–1.35 μm	6	1×300

TABLE 2
Keck/NIRC2 Astrometry of 1RXS J2351+3127 AB

Epoch (UT)	Filter	FWHM (mas)	Strehl	Separation (mas)	PA (°)	Δmag
2011.470	H	39.2 ± 0.5	0.435 ± 0.009	2392.2 ± 2.0	91.77 ± 0.05	5.68 ± 0.04
2011.871	K'	49.0 ± 0.2	0.50 ± 0.02	2386.3 ± 1.5	91.81 ± 0.04	5.04 ± 0.05

Note. — FWHM and Strehl ratios are computed using the publicly available IDL routine `NIRC2STREHL` made available by Keck Observatory.

TABLE 3
Photometry of 1RXS J2351+3127 AB

Property	Primary	Secondary
$R_{\rm USNO-B}$ (mag)	12.28	···
$I_{\rm USNO-B}$ (mag)	10.92	···
$J_{\rm MKO}$ (mag)	9.80 ± 0.02[a]	···
$H_{\rm MKO}$ (mag)	9.21 ± 0.02[a]	14.89 ± 0.04[b]
$K_{\rm MKO}$ (mag)	8.98 ± 0.02[a]	13.92 ± 0.05[b]
$M_{J({\rm MKO})}$ (mag)	6.31 ± 0.46[c]	···
$M_{H({\rm MKO})}$ (mag)	5.72 ± 0.46[c]	11.40 ±0.46
$M_{K({\rm MKO})}$ (mag)	5.49 ± 0.46[c]	10.43 ±0.46
ΔY, IRTF (mag)	5.71 ± 0.19	
ΔJ, IRTF (mag)	5.27 ± 0.27	
ΔH, IRTF (mag)	5.10 ± 0.22	
ΔK_S, IRTF (mag)	4.54 ± 0.12	
GALEX NUV (mag)	19.97 ± 0.09[d]	
GALEX FUV (mag)	21.29 ± 0.26[d]	
ROSAT flux (erg sec^{-1} cm^{-2})	6.4 ± 1.5 ×10^{-13}[c]	
ROSAT HR1	–0.33 ± 0.16[c]	
ROSAT HR2	–0.03 ± 0.30[c]	

[a] Synthetic photometry from our SXD spectrum of 1RXS J2351+3127 A after flux-calibrating it to the 2MASS K_S-band magnitude from Skrutskie et al. (2006).

[b] Computed from our Keck/NIRC2 photometry.

[c] Based on the photometric distance estimate of 50 ± 10 pc.

[d] *GALEX* photometry from GR6 (Morrissey et al. 2007).

[e] From the *ROSAT* All-Sky Survey (Voges et al. 1999). The relation from Fleming et al. (1995) was used to convert count rate to flux.

TABLE 4

Properties of 1RXS J2351+3127 AB

Property	Primary	Secondary
Age (Myr)	50–150[a]	
$d_{\rm phot}$ (pc)	50 ± 10	
Proj. Sep. ($''$)	2.386 ± 0.002	
Proj. Sep. (AU)	119 ± 24	
$\mu_\alpha \cos\delta$ (mas/yr)	105.9 ± 3.5[b]	
μ_δ (mas/yr)	–81.8 ± 5.3[b]	
RV (km/s)	–13.5 ± 0.6[c]	
U (km/s)	–10.5 ± 3.0	
V (km/s)	–29.2 ± 3.7	
W (km/s)	–15.4 ± 4.6	
X (pc)	–13.6 ± 2.7	
Y (pc)	–41.2 ± 8.3	
Z (pc)	–24.8 ± 5.0	
$\log(L_{\rm X}/L_{\rm Bol})$	–3.02[d]	
$\log(L_{\rm Bol}/L_\odot)$	–1.37 ± 0.19	–3.6 ± 0.2
Spectral Type	M2.0±0.5[e]	$\rm L0^{+2}_{-1}$
Mass	0.45 ± 0.05 $M_\odot$	32 ± 6 $M_{\rm Jup}$

Note. — $UVWXYZ$ values are based on the photometric distance estimate. U is positive towards the galactic center.

[a] Assumes the system is a member of the AB Dor YMG.

[b] UCAC-3; Zacharias et al. (2010).

[c] Shkolnik et al. (2012, submitted).

[d] Riaz et al. (2006).

[e] Shkolnik et al. (2009).